heliotek
DIVISION OF TEXTRON ELECTRONICS, INC.
EMPIRE 5-6301
12500 GLADSTONE AVE., SYLMAR, CALIFORNIA
Manufacturer of Space Age Solid State Devices

63-3-3

CATALOGED BY ASTIA
AS AD 402838

HIGH EFFICIENCY SILICON SOLAR CELLS

REPORT NUMBER II

SECOND QUARTERLY PROGRESS REPORT

REPORT DATE: January 15, 1963

PERIOD: September 15, 1962 to December 15, 1962

CONTRACT NO. DA 36-039-SC-90777

ORDER NO. 1091-PM-62-93-93(4213)

PROJECT NO. 3A99-09-002

PLACED BY: U. S. ARMY

ELECTRONICS RESEARCH AND DEVELOPMENT LABORATORY

FORT MONMOUTH, NEW JERSEY

HELIOTEK

DIVISION OF TEXTRON ELECTRONICS, INC.

12500 Gladstone Avenue

Sylmar, California

ASTIA
MAY 6 1963

HIGH EFFICIENCY SILICON SOLAR CELLS

REPORT NUMBER II

Contract No. DA 36-039-SC-90777
Order No. 1091-PM-62-93-93(4213)
Project No. 3A99-09-002

Second Quarterly Progress Report

Covering Period from September 15, 1962 to December 15, 1962

OBJECTIVE: INVESTIGATION FOR THE IMPROVEMENT OF
HIGH EFFICIENCY SILICON SOLAR CELLS
FOR TERRESTRIAL APPLICATIONS

Report Prepared by: Paul A. Berman
Roland J. Handy
Geza P. Rolik

Approved by: Eugene L. Ralph

HELIOTEK
Division of Textron Electronics, Inc.
12500 Gladstone Avenue
Sylmar, California

TABLE OF CONTENTS

TITLE	PAGE NO.
PURPOSE	iii
ABSTRACT	iv
CONFERENCES	v
FACTUAL DATA	1 - 1
1.0 INTRODUCTION AND SUMMARY	1 - 1
2.0 CONCENTRATED SUNLIGHT MEASUREMENTS	2 - 1
3.0 SERIES RESISTANCE EFFECTS AND GRID OPTIMIZATION	3 - 1
4.0 POLYVARIABLE EXPERIMENTS	4 - 1
5.0 COST FACTORS	5 - 1
6.0 ENVIRONMENTAL TESTS	6 - 1
CONCLUSIONS	7 - 1
PROGRAM FOR NEXT INTERVAL	8 - 1
IDENTIFICATION OF KEY TECHNICAL PERSONNEL	9 - 1

PURPOSE

The purpose of this contract is the development of high efficiency, low cost silicon solar cells. The objective is high yields, in the order of seventy (70) percent of the cells having efficiencies in the range of twelve to fourteen percent leading to a cell cost of $2.00 to $3.00 for a cell having dimensions of 1 cm by 2 cm. Both N+ on P and P+ on N cell structures are to be studied and the cells optimized for use in terrestrial environment with and without utilization of solar concentrators.

ABSTRACT

Work on the effect of concentrated sunlight on the performance of solar cells under concentrated solar intensities has been continued. Once again it has been found that the cells which were diffused for twice the length of time as the standard production cells exhibited better performance under 300 mW/cm^2 solar intensity when all other parameters were identical to the standard production-type cells. The series resistance of the former type of cell was several tenths of an ohm lower than the latter type. The P^+/N type cells showed significantly better behavior under concentrated solar illumination than the N^+/P cells, probably due to the lower resistivity material used to fabricate the device.

The actual values of diffused sheet resistance, bulk resistance, contact resistance to the diffused layer electrodes, and contact resistance to the bulk electrodes have been experimentally determined for N^+/P and P^+/N type cells. It was found that the contact resistance at the bulk-electrodes as they are presently fabricated could become appreciable if silicon of greater than 20 ohm-cm resistivity is used as the base material. The contact resistance at the diffused-layer electrode was found to be negligible. A theoretical method has been developed for the determination and isolation of the resistance of the silicon for carriers flowing to the contact strip and for carriers flowing to the grid strip. These resistances can be determined from a knowledge of the resistivity of the diffused sheet and the physical dimensions of the cell.

Cells of N^+/P and P^+/N polarity have been fabricated from polycrystalline base material. Representative spectral response curves are presented. The peak response occurs at a wavelength of about 0.73 microns for the polycrystalline cells where as a normal, single-crystalline cell, regardless of polarity, peaks at about 0.85 microns due to the much higher bulk region minority carrier lifetime. A P^+/N polycrystalline cell having

an efficiency in sunlight (m=1) of greater than 9% has been fabricated. Various diffusion depths and grid patterns are studied with respect to polycrystalline cell performance.

The results of environmental tests on standard production type solar cells are presented.

A polyvariable experiment has been carried out in order to determine the optimum diffusion time and number of grid stripes for fabrication of a P^+/N cell to be operated at a solar intensity of about 300 mW/cm^2.

Experiments to obtain an electroding process which will result in mechanically stronger contacts and lower contact resistances are discussed.

CONFERENCES

On 3 October 1962 a conference was held at the U. S.Army Electronics Research and Development Laboratory, Fort Monmouth, New Jersey. The following personnel were in attendance:

USAERDL:
E. Kittl
G. Hunrath
A. Herchakowski

Representative:
C. Daniel, Statistical Consultant for USAERDL

Heliotek:
M. Wolf
E. L. Ralph

During this conference a polyvariable experiment was designed to statistically analyze both N^+/P and P^+/N type cells with respect to optimization of cell design for application at concentrated solar intensities.

FACTUAL DATA

1.0 INTRODUCTION AND SUMMARY

Two experiments have been performed involving an attempt to obtain information on cell performance at elevated intensities as the series resistance of the cell was varied. The performance of N^+/P and P^+/N cells having various junction depths, under concentrated solar intensities up to about 300 MW/CM^2, were studied. Specifically, cells of each type which were diffused for twice the length of time as standard production cells were compared against cells representative of standard production cells. All other parameters were maintained constant for both cell types, including the number of grid stripes. The deeper diffused cells had series resistances several tenths of an ohm lower than the shallow diffused cell of the same polarity. Results similar to the qualitative results of the First Quarterly Progress Report were obtained; namely, the deeper diffused P^+/N cell exhibited better performance at the higher light levels than the shallow diffused P^+/N cells. Also the P^+/N type cells showed significantly better behavior under concentrated solar illumination than the N^+/P cells, probably due to the lower resistivity material used to fabricate the device. Experiments were performed several months apart and showed excellent reproducibility of results. Work was continued towards analyzing the individual sources of resistance that makes up the total cell series resistance. During this report period actual numerical values have been obtained experimentally for the sheet resistance, bulk resistance, contact resistance at the diffused sheet electrodes and contact resistance at the bulk region electrodes. The values have been obtained for both N^+/P and P^+/N cell types. It was found that the contact resistance at the base electrode could become significantly large so that it would influence the total series resistance of the cell, if the contact was applied to P-type silicon having a resistivity higher than about 20 ohm-cm. However, for P-type silicon having a resistivity of about 4-7 ohm-cm and N-type silicon of about one ohm-cm, the resistance of this electrode is low enough so that it becomes a minor effect. The contact resistance to the diffused layer was found to be negligible for both cell types.

A theoretical method has been developed for the determination of the resistance in the diffused sheet through which carriers must pass when traveling to the contact strip and the grid stripe.

Polycrystalline material has been utilized in the fabrication of both N^+/P and P^+/N solar cells in the hopes of developing a cheaper solar cell. Representative spectral response curves were obtained. The peak response was found to occur at a wavelength of about 0.73 microns for the polycrystalline cells, whereas a normal, single crystalline cell, regardless of polarity, peaks at about 0.85 microns due to the much higher bulk region minority carrier lifetime. Little change in spectral response or short circuit current was observed by applying an anti-reflectance coating to the active surface of a polycrystalline cell. There was also little change in spectral response observed for polycrystalline cells diffused 20 minutes and 45 minutes, though the former type of cells had considerably higher open circuit voltages and efficiencies. The highest efficiency yet observed was greater than 9% in sunlight (M=1), for a P^+/N polycrystalline cell having an eight line grid configuration. This is encouraging, especially in view of the rather short time these cells have been under study.

In order to evaluate and predict the behavior of state-of-the-art solar cells under the environmental conditions to which they may be subjected, an environmental test was carried out and the power degradations at a constant voltage were determined. These will provide a basis for predicting cell behavior under specific environmental conditions.

A bi-variable experiment was undertaken in which the parameters studied were the number of grid lines and the diffusion time, in an attempt to obtain a P^+/N cell which is optimized for operation under concentrated solar intensities of about 300 MW/CM^2. The results of these experiments,

which consisted of ten closely controlled experiments, will be analyzed in a computer program by the USAERDL statistical consultant for determination of the optimum parameters.

2.0 CONCENTRATED SUNLIGHT MEASUREMENTS

Concentrator experiments were continued during this period with particular attention directed towards minimizing the resistance in the test circuit. Series resistance measurements on the cells were made (before and after the cells were soldered to the copper plate) in tungsten light using the method described in the First Technical Summary Report. (This method consists of obtaining the I-V curves of the cell under various light intensities, marking of points on the curve a fixed ΔI back from the short circuit current, and connecting these points with a straight line. The slope of this line is equal to the total series resistance.) No significant change in series resistance was observed after the cells had been soldered to the copper plate indicating that no degradation was introduced because of the mounting process. The use of a copper plate as the cell substrate simplified the cell cooling problem during testing since the copper plate is mounted on a water cooled block and very good heat conduction is achieved. The series resistance as measured in sunlight by the same technique was in good agreement with the measurements made under lower intensity tungsten light thus giving confidence to the measurement. This data is shown in Table I.

Complete current-voltage curves were obtained in sunlight for N^+/P cells, having diffusion times of 20 and 40 minutes and P^+/N cells having diffusion times of 10 and 20 minutes. The short diffusion time for each type cell corresponds to the typical junction depth of a blue sensitive solar cell. The curves were obtained under various levels of illumination from about 100 to 300 mW/cm^2 by utilization of the three mirror solar concentrator system described in the first report.

The cells were mounted on a water-cooled plate and were controlled at constant temperature of 25°C ± 2°C regardless of concentration level. Standard cell readings were taken directly preceding each of the current-voltage measurements. One series of measurements was taken on 21 September, and another on 19 November. The same cells were measured on both days to provide an indication of the reproducibility of the measurements

and the effects of variations of spectral distribution of sunlight on different days. The results of the tests are shown in Table I with the number of mirrors used to concentrate the sunlight being the variable. In the first column the cell identification number is given, while the second and third columns give the maximum power output per mA of the standard cell short circuit current on 21 September and 19 November respectively. This quantity was obtained by dividing the maximum power output, as determined from the current-voltage curve for the cell under test, by the short circuit current of the standard cell. The standard cell was calibrated in sunlight and the short circuit current was determined to be 55.6 mA at 100 mW/cm^2 solar intensity as determined by means of a normal incidence pyrheliometer. The unit solar intensity in this case was 1.8 $mW/cm^2/mA$. The fourth and fifth columns are obtained by dividing the figures in columns two and three by the unit solar intensity of 1.8 $mW/cm^2/mA$, thus basing all the power output data on 1 mW/cm^2 input intensity. These columns are efficiency values if the cell's active area is applied to the figures. Columns six and seven show the total series resistance of the cells before and after mounting on the copper plate as determined in tungsten light, and column eight shows the series resistance of the mounted cells as determined in sunlight at intensities greater or equal to 100 mW/cm^2. The series resistance values obtained under these various conditions compare well with one another.

It can be seen from the figures presented in this table that cell #8, which is a 20 minute diffused P^+/N cell, actually seems to increase in power output per unit solar intensity at the two and three mirror configurations (approximately 200-300 mW/cm^2 solar intensity) over the unconcentrated power per unit solar intensity values. Moreover, the actual power per unit solar intensity values as measured on each of the days are almost identical to one another indicating good reproducibility of results. Cell #8 exhibited the lowest series resistance of the group.

TABLE I

CONCENTRATOR MEASUREMENTS

I	II	III	IV	V	VI	VII	VIII
	Maximum Power 1.8 mW/cm^2 Solar Int.		Maximum Power mW/cm^2		R_s Unmounted Tungsten Light (ohm)	R_s Mounted Tungsten Light (ohm)	R_s Mounted (Sunlight) (ohm)
*Cell No.	9/21/62	11/19/62	9/21/62	11/19/62			
0 MIRROR							
2	.359	.350	.199	.194	.8	.85	.8
1	.375	.362	.208	.201	.6	.6	.5
7	.416	.416	.231	.231	.55	.6	.75
8	.411	.411	.228	.228	.4	.45	.4
1 MIRROR							
2	.354	.351	.197	.195			
1	.372	.376	.206	.208			
7	.416	.419	.231	.233			
8	.415	.426	.230	.238			
2 MIRRORS							
2	.348	.344	.193	.191			
1	.372	.377	.206	.209			
7	.412	.406	.229	.226			
8	.426	.426	.237	.237			
3 MIRRORS							
2	.340	.331	.189	.184			
1	.372	.370	.206	.205			
7	.406	.397	.226	.220			
8	.426	.428	.237	.238			

*Cell No. 2 N^+/P type - 20 minute diffusion time
1 N^+/P type - 40 minute diffusion time
7 P^+/N type - 10 minute diffusion time
8 P^+/N type - 20 minute diffusion time

Cell #2, the shallow diffused N^+/P cell, exhibited the highest series resistance of the group and showed the greatest degradation in maximum power per unit intensity under the more concentrated solar intensities. The possibility that the cell used as a standard gave slightly erroneous readings (due to the fact that it was not in the identical location of the cell being measured), could not be overlooked, although previous equipment checks had shown excellent uniformity of solar intensity over the area utilized in this experiment. Therefore as a check each cell was used as its own "standard" cell: the initial calibration point being chosen at the intensity corresponding to the unconcentrated configuration.

For an intensity increase, the ratio of the standard cell short circuit current at the two intensities should be equal to the ratio of the short circuit currents of the cell under test, providing that both cells are seeing the same intensity shift. This can be easily shown if we consider the standard cell to be cell "a" and the cell being measured as cell "b". The short circuit current is proportional to the incoming solar intensity up to intensities of about 400 mW/cm^2 for most cells. (For a discussion of the limits of the direct proportionality of short circuit current to incoming light intensity see the First Quarterly Report under this contract.) This can be expressed for cell "a" and "b" respectively as:

$$\text{Solar Int.} = C\, I_{sc_a} \quad ; \qquad \text{Eq. (1)}$$

$$\text{Solar Int.} = K\, I_{sc_b} \quad ; \qquad \text{Eq. (2)}$$

where I_{sc_a} and I_{sc_b} are the short circuit currents of "a" and "b" respectively and C and K are constants which are characteristic of the cell. If we consider two levels of solar intensity, $S^{(1)}$ and $S^{(2)}$,

which have identical spectral distributions Eqs. (1) and (2) can be used to yield:

$$\frac{S^{(1)}}{S^{(2)}} = \frac{I_{sc_a}^{(1)}}{I_{sc_a}^{(2)}} = \frac{I_{sc_b}^{(1)}}{I_{sc_b}^{(2)}}$$

Eq. (3)

Equation (3) is valid only if the spectral distributions at the two light levels are identical, since the constants in Eqs. (1) and (2) hold only for a particular energy-wavelength distribution of the incoming light. If the energy wavelength distribution does change at the different intensities, the constants do not cancel out when taking the ratios indicated in Eq. (3) and this equation must be written in the more general form:

$$\frac{S^{(1)}}{S^{(2)}} = \frac{C^{(A)}I_{sc_a}^{(1)}}{C^{(B)}I_{sc_a}^{(2)}} = \frac{K^{(A)}I_{sc_b}^{(1)}}{K^{(B)}I_{sc_b}^{(2)}} \quad ;$$

Eq. (4)

where $C^{(A)}$ and $C^{(B)}$ are the constants associated with cell "a" for a spectral distribution A and B respectively and $K^{(A)}$ and $K^{(B)}$ are the constants associated with cell "b" for a spectral distribution A and B. Since it has been found that during the course of these experiments Eq. (3) is satisfied, which implies that $C^A \equiv C^B$ and $K^A \equiv K^B$, it is unlikely that any significant spectral shift has occured during the course of the measurements.

Columns III and V of Table II present the ratio of the short circuit current at concentrated solar intensities to the short circuit current at the unconcentrated condition for the standard cells and the experimental cells respectively. Excellent agreement was obtained between the two ratios for all readings except for cell #1, and even here the

TABLE II

CONCENTRATOR MEASUREMENTS

I	II	III	IV	V	VI	VII	VIII	IX
*Cell No.	I_{sc} Std. Cell (mA)	Std. (Conc.) / Std. (Unconc.)	I_{sc}	I_{sc} (Conc.) / I_{sc} (Unconc.)	Power Out (Conc.) / Power Out (Unconc.)	**U / Col.VI / Col.V	Maximum Power Output (mW)	Solar Intensity (mW/cm^2)
0 MIRROR								
2	60.0	1.0	57.5	1.0	1.0	1.0	21.0	107.8
1	60.5	1.0	52.0	1.0	1.0	1.0	22.1	108.5
7	60.0	1.0	58.0	1.0	1.0	1.0	25.2	107.8
8	60.0	1.0	57.0	1.0	1.0	1.0	24.7	107.8
1 MIRROR								
2	98.0	1.63	94.0	1.63	1.64	1.01	34.4	176.0
1	98.5	1.63	87.0	1.67	1.67	1.00	37.0	181.0
7	98.0	1.63	94.0	1.62	1.63	1.01	41.1	174.5
8	97.5	1.62	93.5	1.64	1.69	1.03	41.7	176.8
2 MIRRORS								
2	136.0	2.26	130.5	2.26	2.21	.98	46.8	244.0
1	134.0	2.22	120.0	2.31	2.28	.99	50.5	248.0
7	137.0	2.28	130.0	2.24	2.21	.99	55.6	242.0
8	137.0	2.28	130.5	2.29	2.36	1.03	58.5	246.2
3 MIRRORS								
2	174.5	2.91	168.5	2.94	2.74	.93	57.6	315.5
1	174.5	2.88	156.0	3.0	2.92	.97	64.5	322.2
7	175.0	2.92	166.5	2.87	2.76	.965	69.5	310.0
8	174.0	2.90	165.5	2.90	3.02	1.01	74.5	312.2

*Cell No. 2 N^+/P type - 20 minute diffusion time
1 N^+/P type - 40 minute diffusion time
7 P^+/N type - 10 minute diffusion time
8 P^+/N type - 20 minute diffusion time

$$**U \equiv \text{Utilization Factor} \equiv \frac{\text{Power Out (Conc.)}/\text{Power Out (Unconc.)}}{I_{sc}\ \text{(Conc.)}/I_{sc}\ \text{(Unconc.)}}$$

error was only about 4%. The fact that Eq. (3) is satisfied to a good approximation indicates that the solar intensity was quite uniform over the area utilized within the concentrator and that the standard cell can be utilized to determine the incident solar intensity with little or no error due to the positioning of the cells with respect to one another. It also indicates that there was little or no shift in spectral distribution during the time of the measurements.

It should be pointed out here that it has been found experimentally that the relationship between unconcentrated intensity as measured by a pyrheliometer and the short circuit current of a solar cell is not simply a direct proportionality, but that due to a shift in spectral distribution with unconcentrated solar intensity in earth's atmosphere the current-solar intensity relationship exhibits a behavior which is not quite linear. The error associated with such a departure from linear behavior has been found statistically to be about 5% when linear behavior is assumed. These results have been obtained from data taken at Table Mountain, California, and it might be expected that an even larger variation in spectral distribution, and hence a larger error in assuming linear behavior would exist at sea level. Fortunately, such errors do not influence these particular experiments adversely since the relative behavior of the various cell configurations is being studied, the absolute power levels being used only to provide an indication of the solar intensity to within about 10%. Also, the effect of a shift in spectral distribution has not been found to be of concern with respect to reproducibility of measurements as attested to by measurements which were taken two months apart and which reproduced one another with an error of less than 3.5% (see columns IV and V in Table I).

We shall define a utilization factor at any concentrated light level as the ratio of the power output at that light level to the power output at the unconcentrated light level divided by the ratio of the short circuit current of the cell at the concentrated level to the short circuit

current at the unconcentrated level. That is:

$$\text{Utilization Factor} \equiv U \equiv \frac{\text{Power out (Conc.)}}{I_{sc}(\text{Conc.})} \Big/ \frac{\text{Power out (Unconc.)}}{I_{sc}(\text{Unconc.})} \qquad \text{Eq. (5)}$$

The standard cell is then used only to insure that the solar intensity during the performance of the unconcentrated measurement does not vary by more than 2%, and the short circuit current of the experimental cell itself is used as its own standard.

The utilization factor is essentially normalized at the unconcentrated position, and by knowing the utilization factor at any higher intensity the power output at this higher intensity can be obtained by simply multiplying the unconcentrated power output by the utilization factor. This assumes I_{sc} is linear with intensity.

The 20-minute diffused P^+/N cell (Cell #8) actually maintains its utilization value of approximate unity throughout the range of all three mirror concentration steps (approximately 100, 200, and 300 mW/cm^2 incoming solar intensity). The shallow diffused N^+/P cell had the lowest utilization factor (.93) at the three mirror position. The utilization factors for each of the cells at the various light levels are shown in Column VII of Table II.

Figure 2-1 shows graphically the dependence of power output on incoming solar intensity. Cell #8 shows the best behavior under concentrated solar intensities (from 100 to 300 mW/cm^2) with the shallow diffused N^+/P cell showing the poorest behavior. These results were similar to the qualitative results obtained during the first quarter. It is becoming quite clear that the P^+/N cells exhibit better efficiencies under concentrated solar illumination than the N^+/P cells when the cells are fabricated from production-type material.

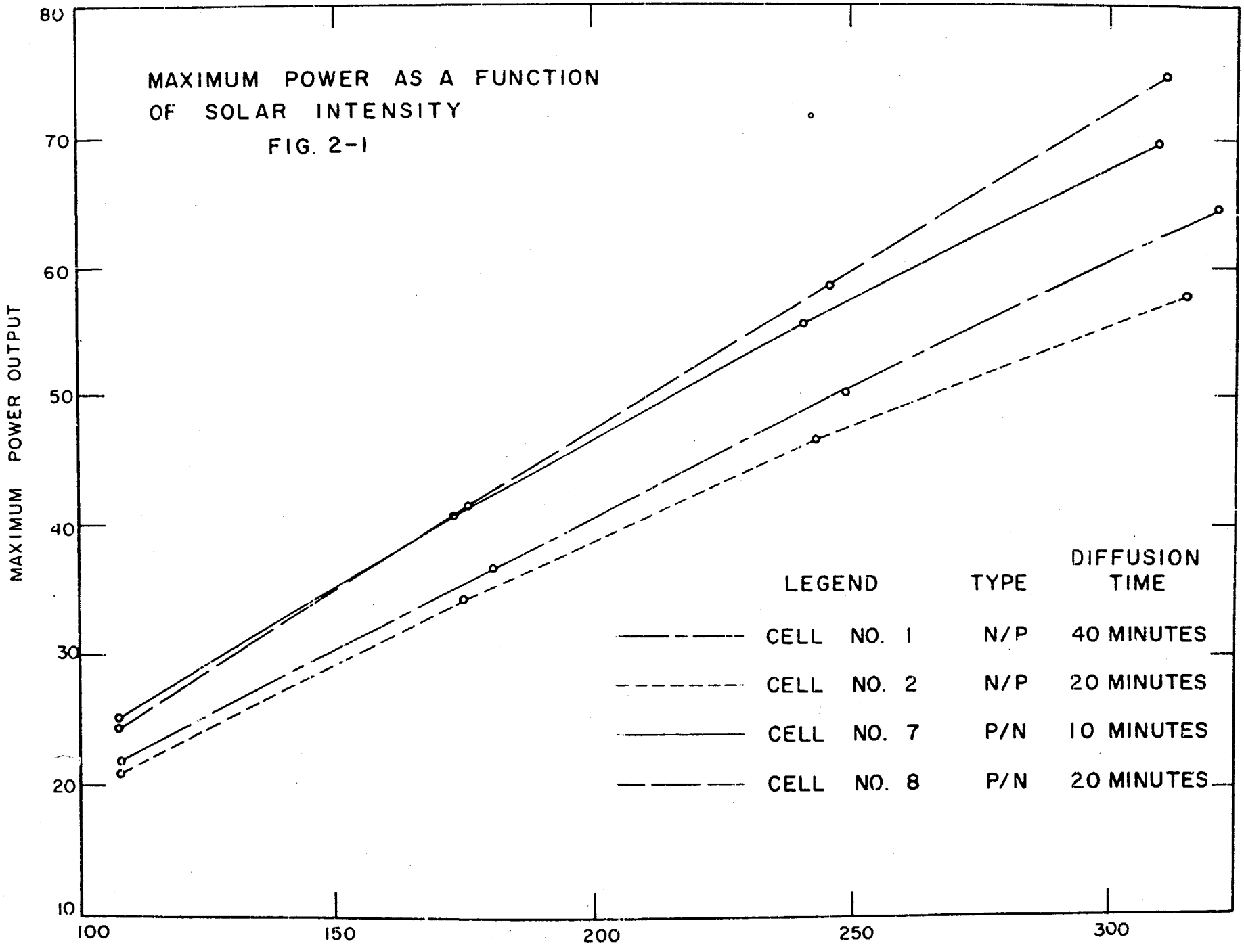
MAXIMUM POWER AS A FUNCTION
OF SOLAR INTENSITY
FIG. 2-1
MAXIMUM POWER OUTPUT
80
70
60
50
40
30
20
10
100
150
200
250
300
LEGEND
TYPE
DIFFUSION TIME
CELL NO. 1
N/P
40 MINUTES
CELL NO. 2
N/P
20 MINUTES
CELL NO. 7
P/N
10 MINUTES
CELL NO. 8
P/N
20 MINUTES

T-2124

The incoming solar intensity was determined by calibrating each of the cells against the standard cell in the unconcentrated condition and using each cell as its own standard for the higher concentration levels. That is, the following equation was utilized to determine the incoming solar intensity for each of the experimental cells:

$$P_{(x)_{in}} \left(\frac{mW}{cm^2}\right) = C \cdot I_{(o)_{std}} \cdot \frac{I_{(x)_{cell}}}{I_{(o)_{cell}}} \left(\frac{mW}{cm^2}\right) ; \qquad \text{Eq. (6)}$$

where $P_{(x)_{in}}$ is the incoming solar intensity at the level x; C is the calibration constant which relates the short circuit current of the standard cell to the incoming intensity as determined with a calibrated pyrheliometer, for the particular spectral distribution as given by Eq. (1); $I_{(o)_{std}}$ is the short circuit current of the standard in the unconcentrated configuration; $I_{(x)_{cell}}$ is the short circuit current of the cell being measured in the unconcentrated configuration. ($I_{(o)_{cell}}$ must be measured at about the same time as $I_{(o)_{std}}$ to insure that the intensity or spectral distribution does not differ.)

The results obtained from this set of experiments are in agreement with the results obtained in the first quarter, the indication being that if all other parameters (including the grid configuration) are kept constant, the cells which are diffused for twice the length of time as standard production type cells show more promise under light levels of about 300 mW/cm^2 than the cells presently in production. Furthermore, the P^+/N cells, which had the lowest series resistance, show better behavior at these intensities than the N^+/P cells. This latter fact is probably due to the lower resistivity base material used to fabircate the P^+/N type cells. During this quarter some N^+/P cells were fabricated from low resistivity (less than 1 ohm-cm) base material but these cells were considerably lower in efficiency than control cells concurrently fabricated from higher resistivity material and are probably not representative of the potential which could be realized from N^+/P cells fabricated from low resistivity material. Cells are presently being fabricated from new low-resistivity P-type material, but have not as yet been processed through and evaluated.

3.0 SERIES RESISTANCE EFFECTS AND GRID OPTIMIZATION

3.1 General

In the First Quarterly Progress Report, a qualitative analysis of the various resistance components in the solar cell was presented, however specific measurements had not yet been made. During this report period, numerical values have been obtained for the sheet resistance, the bulk resistance, the contact resistance at the diffused layer electrode, and the contact resistance at the base electrode for both N^+/P and P^+/N cell types. Also, a theoretical method has been developed whereby the resistance of the diffused sheet to carriers flowing to the contact strip and to carriers flowing to the grid stripe, which are not physically separable and which are equal only for special cases, can be determined through knowledge of the resistivity of the diffused sheet and the physical dimensions of the cell.

A number of experiments have been conducted to isolate the various sources of series resistance in a silicon solar cell and to determine their magnitude. It has been established again that the largest contributions to the series resistance are made by the distributed resistance of the silicon in the diffused sheet, and the resistance of silicon in the base region of the cell. The contact resistance of the semiconductor-metal interface at the base electrode can become appreciable where the base material has a relatively high resistivity (on the order of 20 ohm-cm). A brief discussion of the various experiments and their numerical results follows.

In the first report a model for the equivalent resistance circuit was presented and this model is shown again as a reference in Fig. 3-1 for the following discussion.

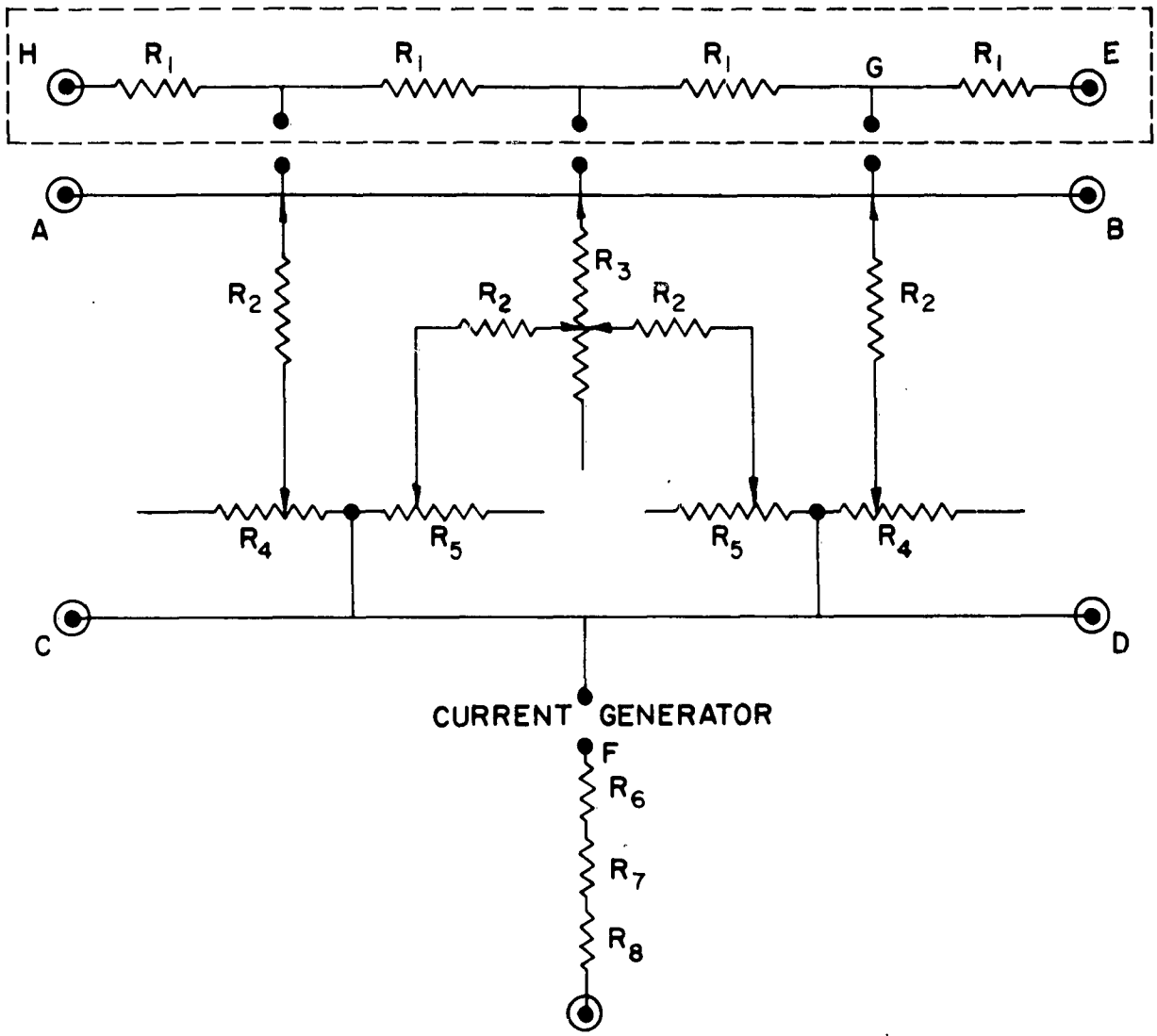

$4R_1$ = Resistance of contact strip
R_2 = Contact resistance between diffused region and electrodes
R_3 = Resistance of grid strip
R_4 = Resistance of diffused region for carriers flowing to contact strip
R_5 = Resistance of diffused region for carriers flowing to grid strip
R_6 = Resistance of bulk region
R_7 = Contact resistance of bulk region to bottom electrode
R_8 = Resistance of bottom electrode

Figure 3-1

3.2 Diffused Sheet Resistance

The resistance of the diffused sheet is commonly expressed in values of "sheet resistance", the dimension of which is ohms, occasionally also called "ohms per square". The sheet resistance represents the resistance of a sheet of the material, of given thickness but having otherwise any dimensions as long as it is rectangular, and as its length equals its width. In this case:

$$R = \frac{\rho \ell}{A} = \frac{\rho \ell}{t} = \frac{\rho}{t} \text{ ohms} \equiv \rho_s \quad ; \qquad \text{Eq. (7)}$$

where ℓ is the length, t is the thickness (in this case the diffusion depth) and ρ is the resistivity of the diffused layer.

Typical sheet resistance for the diffused layer of P^+/N cells is of the order of 24 ohm, while the typical values of sheet resistance for the diffused layer of N^+/P cells are about 40 ohm or higher. The measurements are made by means of a four-point probe, the relationship between current, voltage and sheet resistance ρ_s being:

$$\rho_s = \frac{V}{I} \frac{\pi}{\log_e 2} = \frac{V}{I} \times 3.75 \quad ; \qquad \text{Eq. (8)}$$

for equal probe spacing of .0625".

Through utilization of the expression for R_4 and R_5 (the resistance of the diffused region for carriers flowing to contact strip and for carriers flowing to the grid stripe respectively) which is developed in this report, the sheet resistance and physical dimensions of the cell can be used to determine the magnitude of these two resistances.

3.3 Base Resistance

The resistance of the silicon in the base region is determined from the resistance formula:

$$R = \frac{\rho \ell}{A} \qquad \text{Eq. (9)}$$

where the material resistivity, ρ, is measured by means of a four point probe. Typical values of resistance in the base region for P^+/N and N^+/P cells are .025 ohm and .15 ohm, respectively. The higher base resistance of the N^+/P cells occurs because of the utilization of higher resistivity material.

3.4 Metal-Semiconductor Contact Resistance

The series resistance contributed by the metal to semiconductor contacts on the top and bottom of the solar cell has also been considered. This resistance, unlike the contribution due to the distributed resistance of the diffused layer or the resistance obtained as a result of the width of the grid lines, does not have to be optimized to some value for most efficient operations. Instead the goal is always to obtain the lowest contact resistance possible as long as mechanical, electrical or economic factors are not degraded.

For either the P^+/N or N^+/P type cells the contact resistance to the diffused or degenerate surface has been found to be about an order of magnitude lower than the contact resistance on the back side of the cell for the type material being considered. The contact resistance between the diffused region and the top electrode can be determined experimentally by utilizing a slice doped with the same type impurity as the diffusant and of known resistivity. That is, boron (a P-type dopant) is diffused into P-type material, and phosphorus into N-type material. The resistance of the slice prior to diffusion is determined by means of a four-point probe measurement and Eq. (9). Since the length, ℓ, in this case is about 500μ, and the total depth of diffusion is about 1μ (0.5μ into each face of the slice), the error in the determination of the total slice resistance introduced due to the low resistivity diffused region is negligible ($\sim 10^{-6}$ of the resistance value).

The contacts are then deposited and the total resistance of the slice plus the contacts determined from the current I through it and the voltage drop ΔV across it:

$$R = \frac{\Delta V}{I} \quad ; \qquad \text{Eq. (10)}$$

The resistance of the slice is subtracted from this value and the difference divided by 2 (because contact resistance to both surfaces is being measured). The contact resistances determined in this manner have been found to be negative numbers, -.005 ohm for P-type diffused slices and -.002 ohm for N-type diffused slices respectively. That is, the total slice resistance after the contacts had been applied was measured and found to be lower than the resistance value of the silicon as determined from the resistivity measurement made before the contacts were applied. This apparent decrease in resistance is probably due to errors in obtaining the resistivity of the silicon slice which are estimated to be up to 10%, but serves to show that the contact resistance at the diffused layer contact is small and is about 0.01 ohm for both N^+/P and P^+/N solar cells, which is not significant at this time.

The contact resistance between the base region of the cell and the base electrode has been determined by applying contacts to both sides of a silicon slice of known resistance. The resistance of the silicon slice has been obtained by means of four-point probe resistivity measurements and utilization of Eq. (9). The contacts have been applied by exactly the same methods as normally used for the base contacts of P^+/N or N^+/P silicon solar cells, respectively. The contacts have covered the total of both large surfaces of the wafer, but not its edges. The wafers used were cut from the same types and resistivities of silicon as normally used for the base region of silicon solar cells. They have not contained any p-n junctions. The resistance of the slice with the contacts applied has then been measured and the resistance of the silicon itself mathematically subtracted from this total resistance. The contact resistance equals one-half the value thus obtained. The factor one-half occurs because of the fact that contacts have been made to both sides of the slice. For P-type silicon with a resistivity range of 4 to 7 ohm cm, the contact resistance for the standard nickel plated contacts has been found to be .07 ohm with a standard deviation of .05 ohm. For N-type silicon having a resistivity of about 1 ohm-cm the contact resistance of the standard nickel plated contacts was .08 ohm with no significant standard deviation.

Contact resistances have also been measured on P-type silicon having resistivities of 19 to 24 ohm-cm. It has been found that the contact resistance to this higher resistivity material was .54 ohm with a standard deviation of .49 ohm. This indicates that in special cases the contact resistance between the base region and the base electrode can become significantly large with respect to total resistance of a normal solar cell. The contact resistance increases with increasing resistivity because of the constancy of the Fermi level throughout a system in thermodynamic equilibrium, and because of the fact that the Fermi level of the semiconductor moves towards the center of the forbidden energy gap resulting in a larger potential barrier at the metal-semiconductor interface. Hence, it is important that the resistivity of the base material be maintained relatively low (preferably less than 10 ohm-cm), if low series resistance is desired. Otherwise, a different contacting technique must be used.

Several contacting techniques which are used successfully in various semiconductor processes and which appeared to be applicable for solar cell contacts, were investigated in an attempt to decrease the series resistance of the back contact of the solar cell. The standard nickel plated contact was compared to a fired or sintered nickel contact and a fired or sintered silver-titanium contact. The evaluation technique involved making contact to a silicon blank of the material of interest with no junction present in the manner described above.

As mentioned above the resistance of the contact to N-type (about 1 ohm-cm) material using the standard nickel plated contact is about 0.08 ohm. This can be reduced to about 0.02 ohm by using the fired or sintered nickel type contact. The improvement made by firing is not sufficient to justify a complete process change such as this, since the standard contact resistance is sufficiently low that further effort in this respect is not necessary.

Studies of the contacts to the base of the N^+/P cells show that there is an appreciable contact resistance in certain cases. As mentioned above the standard nickel plated contact on P-type silicon (4 - 7 ohm-cm) has a resistance of about 0.07 ohm while on P-type silicon (19 - 24 ohm-cm) the resistance was about 0.54 ohm. Fired or sintered nickel contacts were put on P-type material (about 10 ohm-cm) for comparison purposes and it was found that the results were not consistent. The contact resistance varied between 0.2 ohm and 0.4 ohms. In any case no improvement was obtained as in the N-type material. After removing the fired nickel from the surface of the P-type material by etching in aqua-regia, it was observed that there were regions on the surface that indicated N-type when a hot point probe measurement was made. Therefore the phosphorus contained in the deposited nickel must be diffusing into the silicon during firing and producing areas which have p-n barriers and giving rise to inconsistent results. As the resistivity increases the effect becomes more pronounced and the contact resistance increases to prohibitive values. Therefore for contact to P-type base material this contacting technique is not advisable.

Contacts made using a fired or sintered silver process were also considered for the P-type base contact. These studies showed that the contact on P-type (7 - 14 ohm-cm) material had a resistance of 0.01 ohm, exhibiting no rectifying behavior and extremely low resistance. Therefore it appears that for the high resistivity base N^+/P cells this contact may be advantageous. Investigations should be made to determine the magnitude of the resultant efficiency increase due to the reduction of contact resistance from about 0.07 ohms or greater to about 0.01 ohm.

3.5 RESISTANCE OF THE DIFFUSED LAYER

Determination of the actual values of the diffused layer resistance R_4 and R_5, of Fig. 3-1 present somewhat of a different problem than the other resistances in the equivalent circuit, since these resistances are not easily separated for individual physical measurement. Also, one must take into consideration the fact that current density in this region is not uniform since current generation occurs over the entire surface, with a subsequent flow to the collecting contacts. The only easily measureable property of this region is the sheet resistance or sheet resistivity which has been discussed in a previous section. It is therefore necessary to develop an expression which accurately describes the resistance of this layer in terms of these measureable quantities (i.e. sheet resistivity and dimensions of the cell unit field).

Referring to Fig. 3-2 it can be seen that the diffused layer can be broken up into identical parts which correspond to a unit field. Within this unit field there are two areas which are symmetrical about the grid line and have dimensions $\frac{S}{2}$ x W. These regions are the basic areas which are repeated throughout the cell and are electrically connected in parallel. If one considers the probability of the generated current paths, the collection of the generated current from areas A and B will be made at the main contact strip and the grid lines respectively. There will be an artificial boundary line formed at an angle θ which separates these areas. The two regions A and B are assumed to be a triangle and trapezoid respectively. The first step in determining the resistance of these areas is to find the electric field developed in the layer due to the current flow.

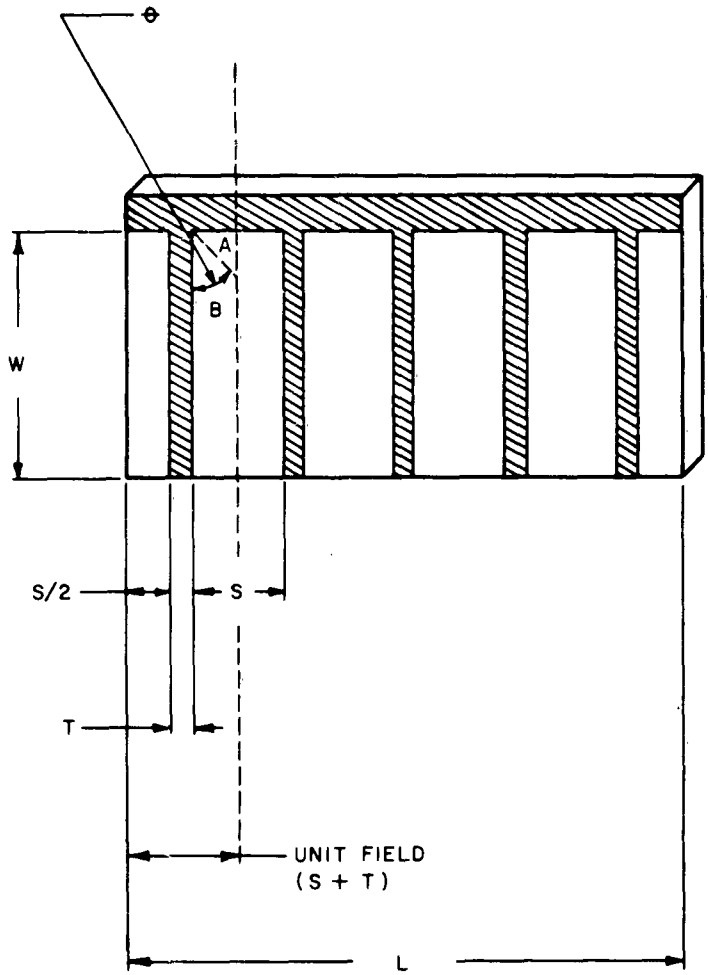

FIG. 3-2

T-2123

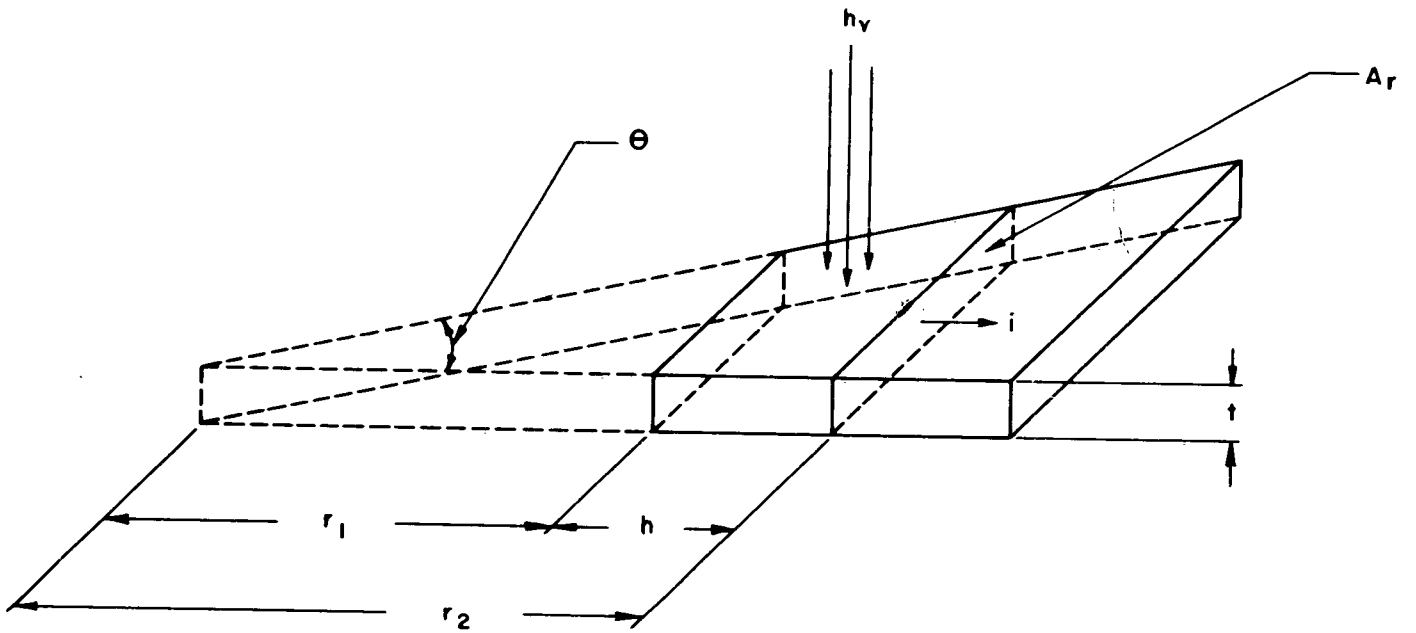

T-2121

FIG. 3-3

Assuming a one-dimensional flow, we have that the electric field is equal to the resistivity times the current density. Thus:

$$\vec{E}_r = \rho \vec{J}_r \quad ;$$

Eq. (11)

where $\vec{E}_r$ and $\vec{J}_r$ are both vector quantities, and ρ (a scalar) being the resistivity of the media.

The total current i_r flowing in the direction of the electric field can be represented by the product of the current density J_r in the direction of the current flow and the area A_r perpendicular to this flow, giving:

$$i_r = (J_r)(r_2 \text{ Sin } \theta)(t) \quad ;$$

Eq. (12)

where t = thickness of media and r_2 Sin θ is the length of the rectangular area A_r, r_2 distance from 0 (the apex). Figure 3 - 3 is a representation of this model and can be used for analyzing both the triangle and the trapezoid regions, the trapezoid being a special case of the triangle.

The amount of current (i_r) flowing in the radial direction is a function of the light intensity incident on the surface of the solar cell, and from the continuity equation we have:

$$i_n = i_r \quad ;$$

Eq. (13)

where i_n = current produced by photon absorption at steady state conditions in the normal direction to the surface of the cell.

Since, in general, the total current i is equal to the product of the current density J times the area A through which the current is flowing,

Eq. (13) can be put in the form:

$$J_n A_n = J_r A_r \quad ;$$

or

$$J_n A_n = (J_r)(r_2 \text{ Sin } \theta)(t) \quad ; \qquad \text{Eq. (14)}$$

where J_n is the generated current density in the normal direction and A_n is the area normal to this current density. A_n is always taken to be that area which lies to the left of the area A_r. From Fig. 3-3 we have:

$$A_n = \frac{1}{2} h(r_1 + r_2) \text{ Sin } \theta \quad ; \qquad \text{Eq. (15)}$$

and since $h = r_2 - r_1$ we have:

$$J_r = \frac{J_n(r_2^2 - r_1^2)}{2 r_2 t} \quad ; \qquad \text{Eq. (16)}$$

from the substitution of A_n into Eq. (14). This equation represents the current density flowing in the radial direction as a function of current density generated in the normal direction. The substitution of Eq. (16) into Eq. (12) gives:

$$i_r = \frac{J_n(r_2^2 - r_1^2) \text{ Sin } \theta}{2} \quad ; \qquad \text{Eq. (17)}$$

which represents the current flowing in the radial direction as a function of the light generated current density J_n.

The substitution of Eq. (16) into Eq. (11) gives:

$$\vec{E}_r = \rho \frac{\vec{J}_n(r_2^2 - r_1^2)}{2 r_2 t} \qquad \text{Eq. (18)}$$

This gives the value of the electric field $\vec{E}_r$ as a function of r_2, r_1 and J_n.

The potential that is produced by an electric field may be calculated from:

$$\Phi = \int_{\text{path}} \vec{E} \cdot d\vec{r} \quad ; \qquad \text{Eq. (19)}$$

where $d\vec{r}$ represents the path over which the field exists. By substitution of Eq. (18) into (19) we can calculate the potential that will exist in the media due to the field produced by the light generated changes. The potential Φ is given by:

$$\Phi = \frac{\rho J_n}{2t} \left\{ \int_{r_1}^{r_2} r_2 dr_2 - \int_{r_1}^{r_2} \frac{r_1^2 \, dr_2}{r_2} \right\} \qquad \text{Eq. (20)}$$

This represents the general equation for the potential.

In the determination of the resistance R_5, r_1 will be equal to a constant and r_2 the variable of integration. The potential equation then takes the form:

$$\Phi_{R_5} = \frac{\rho J_n}{2t} \left\{ \int_{r_1}^{r_2} r dr - r_1^2 \int_{r_1}^{r_2} \frac{dr}{r} \right\} \qquad \text{Eq. (21)}$$

In the determination of the resistance R_5, r_1 will be equal to zero and the variable of integration will be r_3 (see Fig. 3-3). This is done so that one will be reminded that the limits of integration are different in the determination of R_4 and R_5. This gives us the potential equation for R_4:

$$\Phi_{R_4} = \frac{\rho J_n}{2t} \int_0^{r_3} r \, dr \qquad \text{Eq. (22)}$$

In determining the limits for Eq. (21) and Eq. (22) one could assume that

R_4 is a right 45° triangle, but this would be a false assumption since there is no guarantee that current flow is not taking place between R_4 and R_5. It would be more appropriate to let the potential ΦR_4 and ΦR_5 be equal at the point P (see Fig. 3-4) and solve for the limits of integration, by solving these equations in terms of one variable, such as r_3. That is, find r_1 and r_2 in terms of r_3 and solve for the r_3 which makes the potential ΦR_4 and ΦR_5 equal at the point P, thus guaranteeing no current flow between R_4 and R_5. From Fig. 3-4 we get the following relationships: $r_1 = \frac{S(W-r_3)}{2\,r_3}$ and $r_2 = \frac{SW}{2\,r_3}$ and upon the substitution of these limits into Eqs. (21) and (22), we get the following potential equation in terms of one variable r_3.

$$\Phi_{R_5} = \frac{J_n}{2t}\left\{\int_{\frac{S(W-r_3)}{2\,r_3}}^{\frac{SW}{2r_3}} r\,dr - \frac{S^2(W-r_3)^2}{4\,r_3^2}\int_{\frac{S(W-r_3)}{2\,r_3}}^{\frac{SW}{2r_3}} \frac{dr}{r}\right\} \qquad \text{Eq. (23)}$$

and

$$\Phi_{R_4} = \frac{\rho J_n}{2t}\int_0^{r_3} r\,dr \qquad \text{Eq. (24)}$$

Upon integrating Eqs. (23) and (24) and letting $\Phi_{R_4} = \Phi_{R_5}$ one gets:

$$\left(\frac{2\,r_3}{S}\right)^2 = \frac{2W}{r_3} - 1 - 2\left(\frac{W}{r_3} - 1\right)^2 \log\left(\frac{W}{W-r_3}\right) \qquad \text{Eq. (25)}$$

The graphical method was used in the determination of numerical values for r_3 from this transcendental equation (Eq. (25)). The values of r_3 for constant W and for different values of S (grid stripes)

T-2085

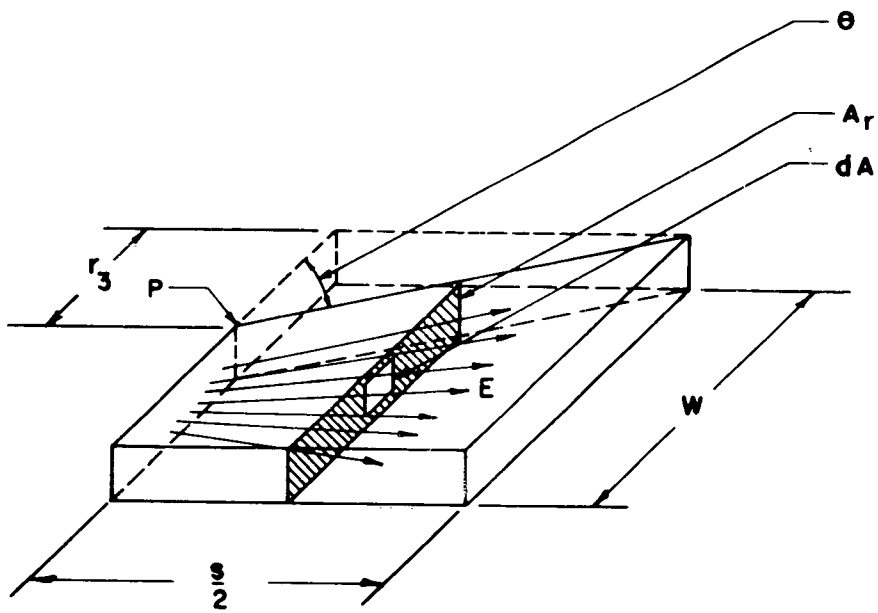

FIG. 3-4

are given in Table III. Also given are the values of the angle θ (see Fig. 3-4) determined by the computed r_3 values.

TABLE III

Case	r_3 (cm)	S (cm)	W (cm)	θ
1	.5	$\frac{2}{3}$	.9	33°41'
2	.37	$\frac{2}{5}$	.9	28°24'
3	.286	$\frac{2}{7}$	.9	26°34'
4	.24	$\frac{2}{9}$	.9	24°51'

The value of resistance of any configuration, by Ohm's law, is equal to the total potential existing across the configuration divided by the total current flowing through it.

The total current flowing through the section represented by the resistance R_5 is:

$$i_r = i_n = J_n A_n \quad ;$$

which is, in terms of r_3:

$$i_r = i_n = J_n \left(\frac{S}{4}\right)(2W - r_3). \qquad \text{Eq. (26)}$$

Thus the value of R_5 from Eqs. (23) and (26) is from the above definition.

$$R_5 = \frac{2\rho}{St(2W-r_3)} \left\{ \int_{\frac{S(W-r_3)}{2r_3}}^{\frac{SW}{2r_3}} r\,dr - \frac{S^2(W-r_3)^2}{4r_3^2} \int_{\frac{S(W-r_3)}{2r_3}}^{\frac{SW}{2r_3}} \frac{dr}{r} \right\} \qquad \text{Eq. (27)}$$

The total current flowing through the section represented by resistance R_4 is:

$$i_r = i_n = Jn\left(\frac{Sr_3}{4}\right)$$

Eq. (28)

The value of R_4 can be obtained from Eqs. (24) and (28) and is:

$$R_4 = \frac{2\rho}{St\ r_3} \int_0^{r_3} r\ dr$$

Eq. (29)

The above expressions for R_5 and R_4, Eqs. (27) and (29), are the desired expressions which describe the resistance as a function of the configuration only.

In the above analysis it should be remembered that it was assumed that the electric field $\vec{E}_r$, was in the same direction as the path $d\vec{r}$. This implies that the expression for the potential:

$$\phi = \int_{path} \vec{E} \cdot d\vec{r}\ ;$$

Eq. (30)

can be represented by:

$$\phi = \int_{path} E\ dr$$

Eq. (31)

Since the field $\vec{E}r$ is not the direction of the path then the potential should be expressed as:

$$\phi = \int_{path} E\ \mathrm{Cos}\ \theta\ dr$$

Eq. (32)

If one were to express Eq. (32) as a function of only one variable, the function of integration would become too complex due to the geometry of the configuration. A much simpler method is to find the extremal values the integral can acquire. This is accomplished by taking the Cos Θ out of the integral sign, giving for the potential:

$$\Phi = \text{Cos } \Theta \int_{\text{path}} E \, dr \qquad \text{Eq. (33)}$$

The values of Θ will vary between $\Theta = 0°$ and $\Theta = \Theta_i$ where (i=1,2,3,4) represents the different Θ values in Table III for each case, i.e., Θ_1 = Θ value for case 1, which is equal to 56°19' from Table III and so forth for each case.

Thus from Eq. (33) the values of R_4 and R_5 will lie between the following values:

$$(\text{Cos } \Theta_i)\left(\frac{2\rho}{St(2W-r_3)}\right)\left\{\int_{\frac{S(W-r_3)}{2r_3}}^{\frac{SW}{2r_3}} r\,dr - \frac{S^2(W-r_3)^2}{4r_3^2}\int_{\frac{S(W-r_3)}{2r_3}}^{\frac{SW}{2r_3}} \frac{dr}{r}\right\} \leq R_5 \leq \left(\frac{2\rho}{St(2W-r_3}\right)$$

$$\left\{\int_{\frac{S(W-r_3)}{2r_3}}^{\frac{SW}{2r_3}} r\,dr - \frac{S^2(W-r_3)^2}{4r_3^2}\int_{\frac{S(W-r_3)}{2r_3}}^{\frac{SW}{2r_3}} \frac{dr}{r}\right\} \qquad \text{Eq. (34)}$$

and:

$$(\text{Cos } \theta_i)\left(\frac{2\rho}{\text{Str}_3}\right)\int_0^{r_3} r\,dr \leq R_4 \leq \frac{2\rho}{\text{Str}_3}\int_0^{r_3} r\,dr \quad ;$$

Eq. (35)

where again θ_i (i=1,2,3,4) represents the different θ values from Table III for each grid stripping case.

Since the integral on the left and right side of Eq. (34) is equal to integral on the left and right side of Eq.(35), (this is because of the potential function being equal) we can write Eq. (34) in a much simpler manner, that is:

$$(\text{Sin } \theta_i)\left(\frac{2\rho}{\text{St}(2W-r_3)}\right)\int_0^{r_3} r\,dr \leq R_5 \leq \frac{2\rho}{\text{St}(2W-r_3)}\int_0^{r_3} r\,dr$$

Eq. (36)

When the appropriate values of r_3, S, θ_i, and W from Table III are substituted into Eqs (35) and (36), and given the sheet resistance $\left(\frac{\rho}{t}\right)$ which for a N^+/P cell is 40 while that of a P^+/N cell is 24, the maximum values of R_4 and R_5 are shown in Table IV for the number of grid stripes used.

TABLE IV

	N^+/P		P^+/N	
Case	R_5	R_4	R_5	R_4
1	11.5 Ω	30 Ω	6.93 Ω	18 Ω
2	7.98 Ω	30.8 Ω	4.78 Ω	18.5 Ω
3	7.55 Ω	40 Ω	4.53 Ω	24 Ω
4	6.66 Ω	43.3 Ω	3.98 Ω	25.9 Ω

4.0 POLYVARIABLE EXPERIMENTS

In order to establish a trend of solar cell performance at higher levels of illumination as a function of certain solar cell parameters, a polyvariable experiment was undertaken during this report period. This experiment was discussed in a conference at USAERDL and it was decided to study both N^+/P and P^+/N type solar cells, using a statistically designed experiment in conjunction with a computer analysis of results. The variable parameters which have the greatest influence on cell series resistance were considered. It was decided that of the solar cell parameters affecting cell series resistance (grid design, junction depth, contact resistance, cell size, and bulk resistivity) the most significant and logical parameters to observe in a polyvariable experiment would be grid design and junction depth.

It is quite obvious that fabrication of electrodes having the lowest contact resistance is an optimum situation. It can only be obtained by the development of a new contact deposition process. Since the lowest contact resistance obtainable is desired, it therefore would not be applicable to a polyvariable experiment. For the polyvariable experiment then, the best contact available within the state-of-the-art was used, and a separate study was made to improve this contact. Since the basic goal of the contract is to develop solar cells having the standard dimensions of 1 x 2 cm^2, dimensional variations in cell size were not undertaken in this series of experiments. Should time permit, however, it is possible that other cell configurations and sizes that have potential for decreasing series resistance will be studied during the course of this contract.

Studies in past years have been made on the effect of base resistivity on solar cell performance for P^+/N cells, and the optimum base resistivity material for highest efficiencies at normal sunlight intensities is presently in use. Higher resistivity material has been used in the

fabrication of N^+/P cells with the subsequent sacrifice of some initial efficiency in order to obtain cells having higher radiation tolerance for space applications. The experiments done to date utilizing concentrated solar illumination show that the N^+/P type cells fabricated from higher resistivity base material are much poorer in performance than the P^+/N cells. The main reasons for this are the higher sheet resistances of the diffused layer and the higher base resistance. The effect of the high base resistance can be reduced for this program by using lower resistivity base material, preferably less than 1 ohm-cm, since there is no radiation resistance requirement. As in the case of the contact resistance, this variable would not lend itself to a polyvariable experiment since it is already known that the optimum starting material would be of the lowest resistivity which would still produce high efficiency solar cells. This resistivity would be in the 0.1 to 1.0 ohm-cm range since material of much lower resistivity has too low a minority carrier lifetime to yield high efficiency cells.

Thus, the polyvariable experiment is reduced basically to a bi-variable experiment involving diffusion time (junction depth) and the number of grid stripes as the variables.

It should be noted that it is important to reduce the number of experimental points on an experiment such as this. For each data input all variables except the ones being studied must be kept constant in order to observe the effect on the paramater which is to be optimized. For a semiconductor device such as the solar cell there are many other variables which can completely mask the effect of varying the junction depth and grid spacing. Variations in starting material (silicon crystal), processes (diffusion, plating, etching, etc.) or testing must all be minimized in order for the experiment to be meaningful. For this reason the complete experiment for P^+/N type cells was run and repeated using only one single crystal silicon ingot as the starting material. Special attention was then paid to the processing so that a minimum of breakage or process variations was experienced. Diffusion

effects were minimized by splitting diffusion lots into two groups which were then processed with different grid spacings thus making it possible to see only the influence of the grid spacing as a variable. Repeat runs of each of the points of the octagon matrix were made to add confidence to the results obtained.

Prior to the start of the experiment evaluations of the ingot were made to insure that the ingot was representative of the state-of-the-art ingots used in solar cell fabrication. All slices used in the bi-variable experiment were selected from the same ingot. The diffusion furnaces were profiled periodically to insure constant diffusion temperature for all runs of the experiment.

At the conference at USAERDL an experimental matrix was set up as shown in Fig. 4 - 1 which gives adequate information about the system with a minimum of experimentation. The variables represent a two dimensional surface, and the performance criterion, which for these experiments is power output per unit solar intensity input at intensities of 100, 163, and 316 mW/cm^2, represents a third dimension. This results in the generation of a three dimensional surface. For the solution of the problem one then seeks a peak on the three dimensional surface, or a tendency towards a peak, in order to determine the optimum values of the parameters. The most efficient distribution of points in the two dimensional bi-variable surface is such that the points most closely approach a circle at the periphery of the surface with several points located in the center. For a ten-experiment series the figure would then have an octagonal shape with two experiments directly in the middle as shown in Fig. 4 - 1. Each "X" on the diagram represents an experiment of 10 cells having the parameters shown on the ordinate and abscissa. The slices were taken from the same ingot and all parameters other than the ones being studied were maintained to as close a degree of consistency as possible.

MATRIX REPRESENTATION OF POLYVARIABLE EXPERIMENT FOR P^+/N CELLS

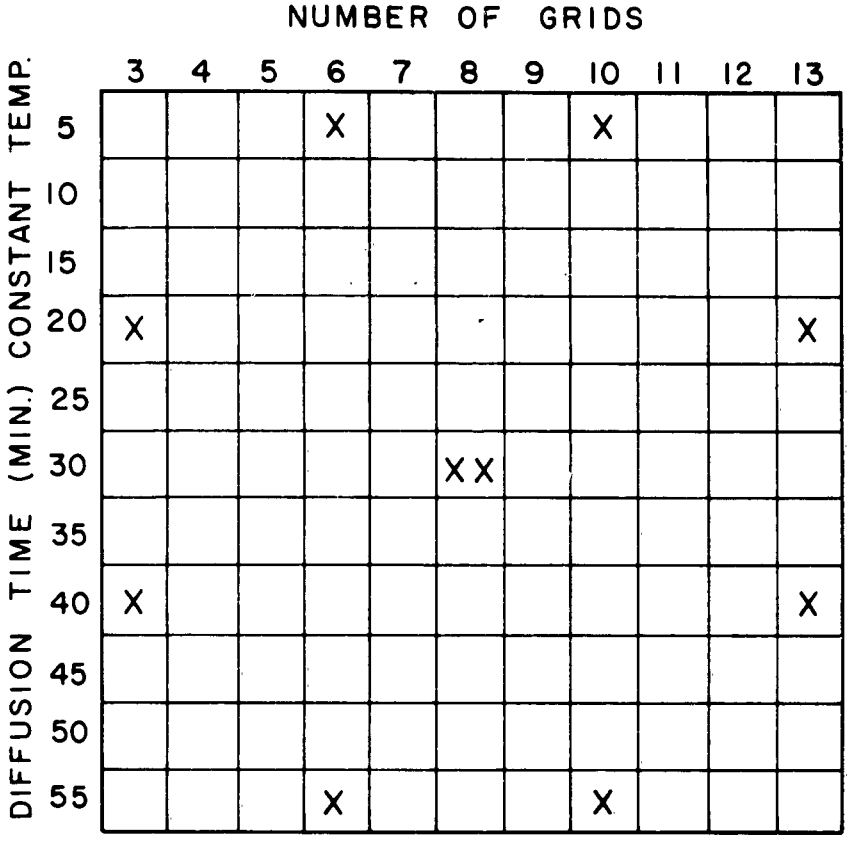

FIG. 4-1

T-2122

Actual measurements were made under tungsten light having a color temperature of 2800°K and the cells were maintained at a temperature of 28°C ± 2°C by means of a water-cooled block. Tungsten measurements were used instead of sunlight because the stability and convenience of this type light source is extremely good and the same information can be obtained if the spectral difference is taken into consideration. The incoming intensity was varied by changing the distance between the cell and the light thus keeping the spectral distribution of the tungsten source constant during the tests. Complete current voltage curves were obtained for each of the cells and for each of the three intensity levels utilized. The cell power output per unit of power input was the merit factor chosen for comparative purposes. Since the cells are to be designed for use in sunlight the power output had to be based on an input having the sunlight spectral distribution. This can be done by determining the relationship or equivalent intensity of the tungsten light source with respect to sunlight for each cell.

Initially the tungsten light was adjusted to correspond to 100 mW/cm^2 solar equivalent by means of three standards whose spectral responses were approximately representative of the experimental cells. The tungsten light, however, will have an equivalent solar intensity of 100 mW/cm^2 only for cells which have the same spectral response as the cells which were used as calibration standards for the tungsten light level, due to the discrepancy in the spectral distributions between sunlight and tungsten light. Cells which have more blue response than the calibration standard will see a lower equivalent solar intensity than the standard, while cells which have more red response will see a higher equivalent solar intensity.

This means that if one were to test all the cells of the experiment in tungsten light and the intensity equivalent to sunlight were to be held constant, the intensity of the tungsten light would have to be adjusted for each cell tested. This would be very complicated and time consuming.

Therefore the actual measurement procedure was as follows. The tungsten light level was set to some intensity near the desired level and this level was held constant while all the cells were tested. The result was that the input intensity equivalent to sunlight was slightly different for the different cells. The data from each cell was then corrected by extrapolation to a common solar intensity for comparison purposes.

To determine the equivalent intensity of sunlight for each cell, the same technique as described in the "Concentrated Sunlight Measurements" section was used. A calibration of each cell was made in sunlight at a known intensity of sunlight as determined by a pyrheliometer. The short circuit current was measured and the ratio of the intensity S* (calibrating intensity) in mW/cm^2 was divided by the calibration short circuit current I_{sc}* in mA, to determine the unit solar intensity C* in $mW/cm^2/mA$. Therefore, each mA of short circuit current corresponds to some sunlight intensity level.

The intensity $S^{(1)}$ (equivalent to sunlight) of any light source can then be determined simply by multiplying the unit solar intensity of the cell by the short circuit current $I_{sc}{}^{(1)}$ of the cell as obtained in this particular light source (1). That is:

$$S^{(1)} = C^* I_{sc}{}^{(1)} = \frac{S^*}{I_{sc}{}^*} I_{sc}{}^{(1)}$$

Eq. (37)

The cell maximum power output per unit of power input or merit factor F is then:

$$F = \frac{P^{(1)}}{S^{(1)}}$$

Eq. (38)

where $P^{(1)}$ is the maximum power of the cell taken from the EI curve obtained in the light source (1).

For evaluation purposes, however, it is much more convenient to express the cell efficiencies at the same intensity, rather than at many different intensities, which would be the result if the above method were utilized unless the light level were changed for each measurement to correspond to the desired solar equivalent intensity. Therefore, the method actually employed in the evaluation was to extrapolate all the maximum power values a small amount so that they all corresponded to the same equivalent solar intensity. This can only be done over small intensity ranges without error. In this study a cross check of the two methods was made and no significant discrepancy in the results was found at any of the intensity levels studied. This was due to the careful selection of the standard which was closely representative of the cells tested. The basic assumption that was used was that the following holds true for a particular cell:

$$\frac{P}{P'} = \frac{I_{sc}}{I_{sc'}}$$

Eq. (39)

where P is the maximum power output of the cell at one intensity and P' is the maximum power output of the cell at a second intensity and I_{sc} and $I_{sc'}$ are the short circuit currents respectively. This implies that the power output increases or decreases exactly as the short circuit current of the cell, which will be true only if the intensities involved are not greatly disproportionate. Otherwise, as was pointed

out in the concentrated sunlight measurements section of this report, significant errors can occur. The equivalent solar intensities from cell to cell varied from the calibrated tungsten intensities as set up by the standard cells by approximately ± 10%. Therefore, it would be expected that Eq. (39) would apply. This was verified through actual computation utilizing the data obtained in the experiments. The power per unit of solar intensity or merit factor was then obtained from each cell at each intensity from the following equation:

$$F_b = \frac{P_b^{(1)} \cdot \dfrac{I_{sc_b}^*}{I_{sc_b}^{(1)}}}{C_a^* \, I_{sc_a}^{(1)}} \qquad \text{Eq. (40)}$$

where: C_a^* is the unit of solar intensity of the standard cell "a" used to set up the tungsten light source (1) and $I_{sc_a}^{(1)}$ is the short circuit current of cell "a" in this source. $I_{sc_b}^*$ and $I_{sc_b}^{(1)}$ are the short circuit currents in sunlight and tungsten respectively of the experimental cell being measured.

The tungsten light was set up by means of the standard cells to the solar equivalent intensities of 100, 163, and 316 mW/cm^2, and the power per unit intensity was determined for each cell based on these same intensities. The results are shown in Figs. 4-2 to 4-9. Straight lines are drawn connecting the experimental points since only three points were obtained for each cell, thus leaving the shape of the curve undefined. The right hand ordinate presents the efficiency based on a 2 cm^2 total area. The experimental points on Figs. 4-2 to 4-5 were determined from the average value of P_{max}/mW for each group while the points on Figs. 4-6 to 4-9 were determined from the P_{max}/mW for the best cell of each group. The latter group of figures are probably a more realistic representation of the potential of the various cell types, since the former figures most likely include variations in processing. The run numbers correspond to the following diffusion times:

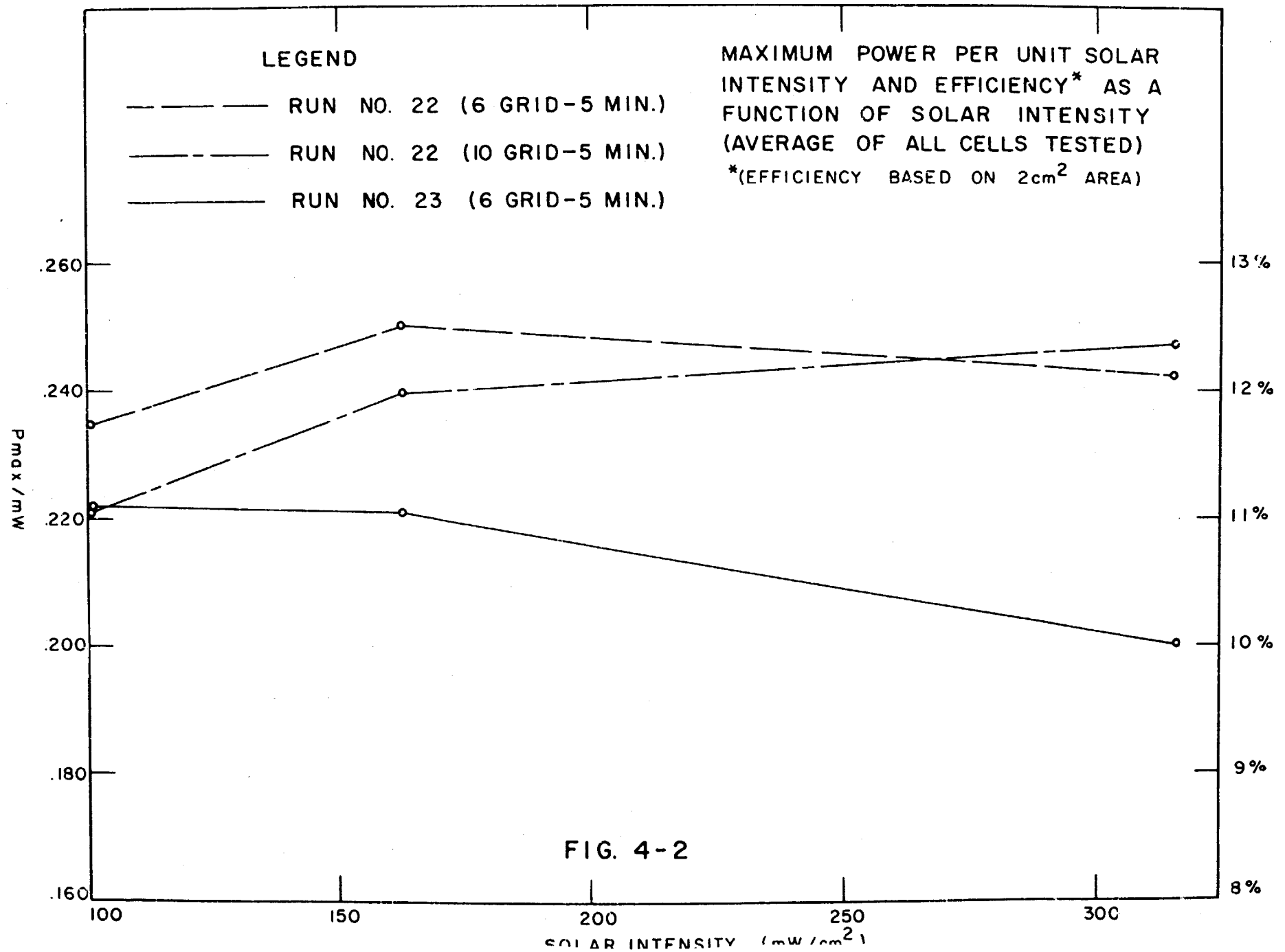
LEGEND
RUN NO. 22 (6 GRID-5 MIN.)
RUN NO. 22 (10 GRID-5 MIN.)
RUN NO. 23 (6 GRID-5 MIN.)
MAXIMUM POWER PER UNIT SOLAR INTENSITY AND EFFICIENCY* AS A FUNCTION OF SOLAR INTENSITY (AVERAGE OF ALL CELLS TESTED)
*(EFFICIENCY BASED ON 2cm² AREA)
.260
.240
.220
.200
.180
.160
Pmax / mW
13%
12%
11%
10%
9%
8%
EFFICIENCY (%)
100
150
200
250
300
SOLAR INTENSITY (mW/cm²)

FIG. 4-2

T-2111

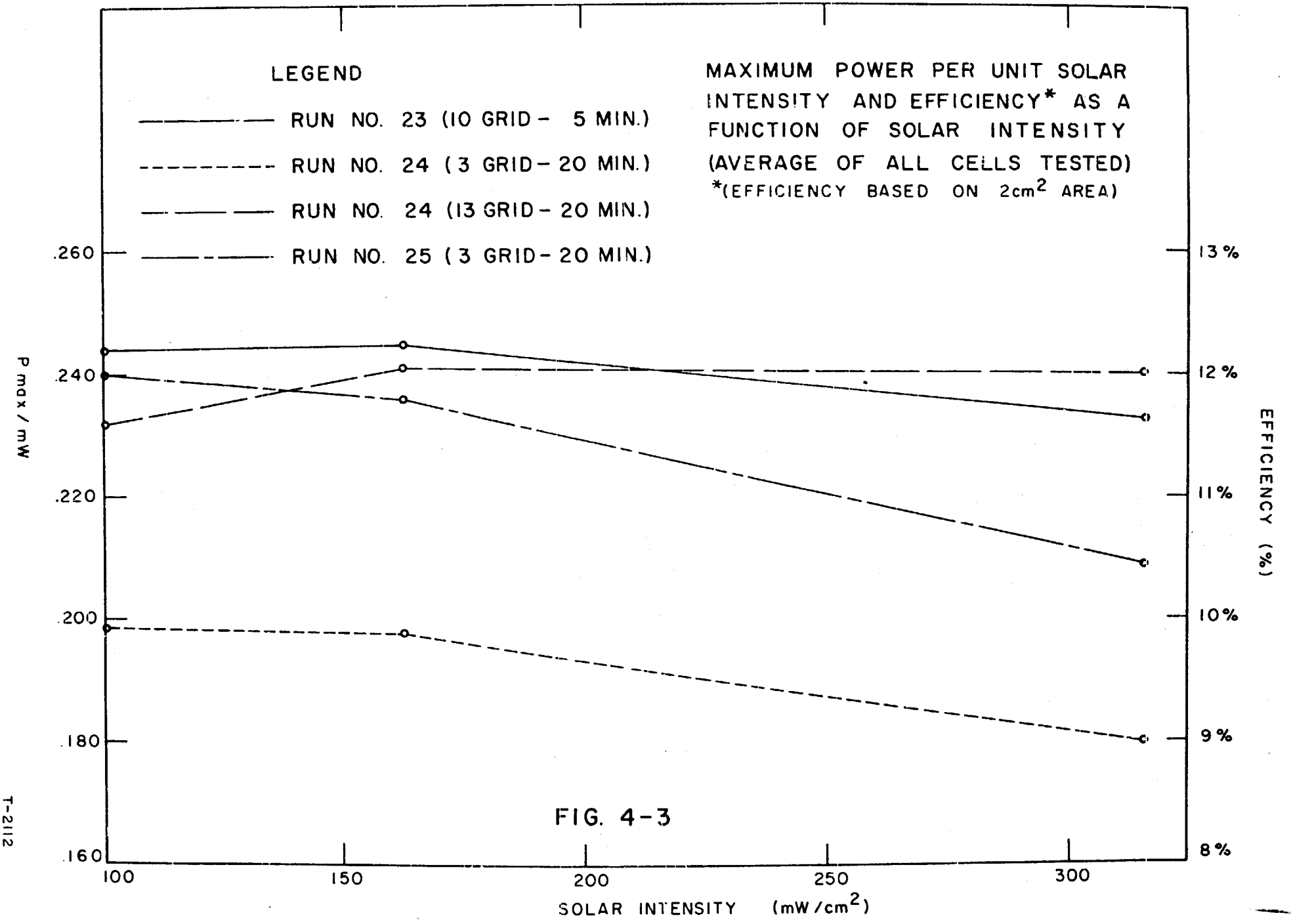
LEGEND
RUN NO. 23 (10 GRID - 5 MIN.)
RUN NO. 24 (3 GRID - 20 MIN.)
RUN NO. 24 (13 GRID - 20 MIN.)
RUN NO. 25 (3 GRID - 20 MIN.)
MAXIMUM POWER PER UNIT SOLAR INTENSITY AND EFFICIENCY* AS A FUNCTION OF SOLAR INTENSITY (AVERAGE OF ALL CELLS TESTED)
*(EFFICIENCY BASED ON 2cm² AREA)
.260
.240
.220
.200
.180
.160
P max / mW
13%
12%
11%
10%
9%
8%
EFFICIENCY (%)
100
150
200
250
300
SOLAR INTENSITY (mW/cm²)

FIG. 4-3

T-2112

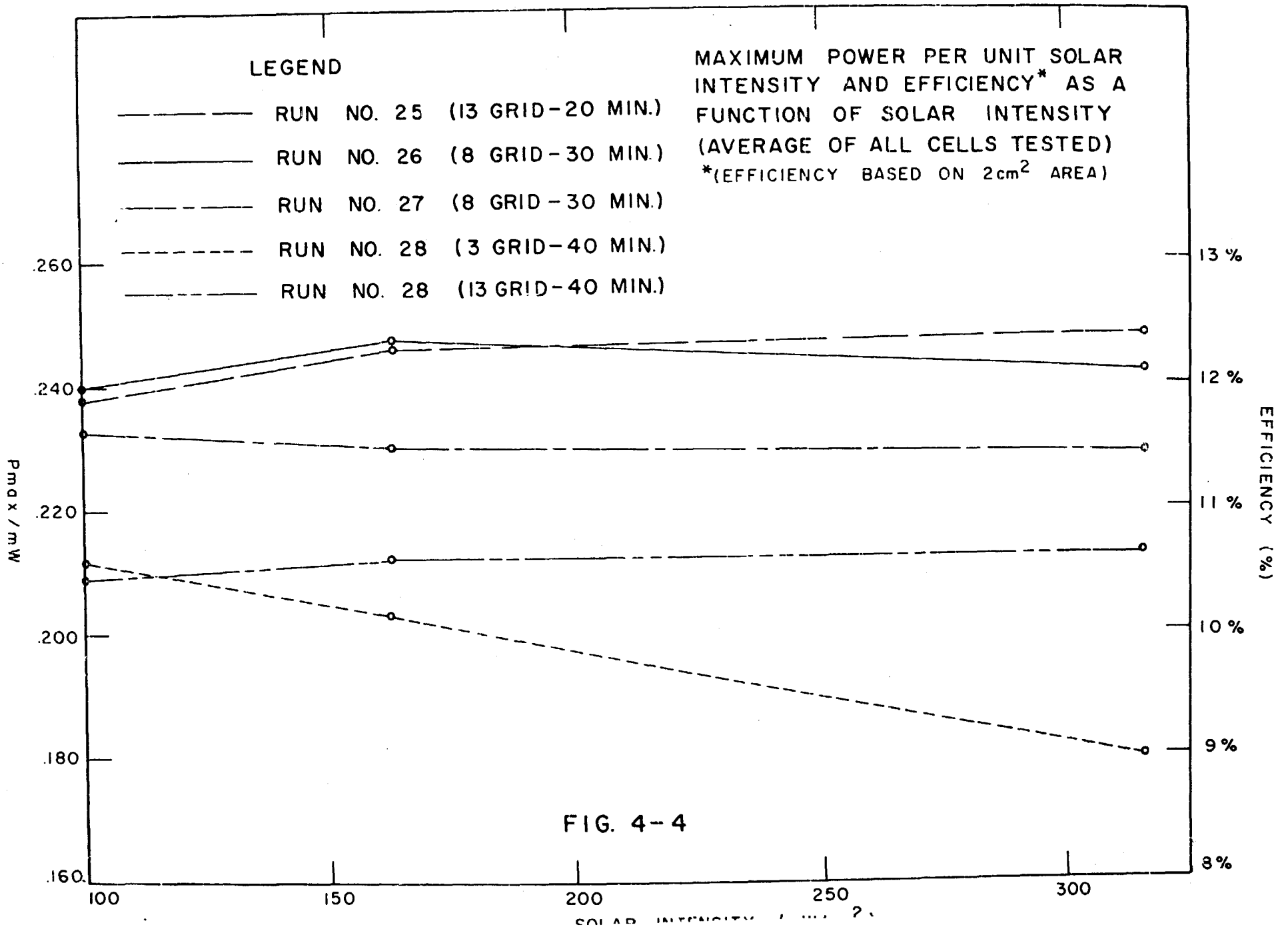
LEGEND
RUN NO. 25 (13 GRID-20 MIN.)
RUN NO. 26 (8 GRID-30 MIN.)
RUN NO. 27 (8 GRID-30 MIN.)
RUN NO. 28 (3 GRID-40 MIN.)
RUN NO. 28 (13 GRID-40 MIN.)
MAXIMUM POWER PER UNIT SOLAR INTENSITY AND EFFICIENCY* AS A FUNCTION OF SOLAR INTENSITY (AVERAGE OF ALL CELLS TESTED)
*(EFFICIENCY BASED ON 2cm² AREA)
.260
.240
.220
.200
.180
.160
Pmax / mW
13 %
12 %
11 %
10 %
9 %
8 %
EFFICIENCY (%)
100
150
200
250
300

FIG. 4-4

T-2113

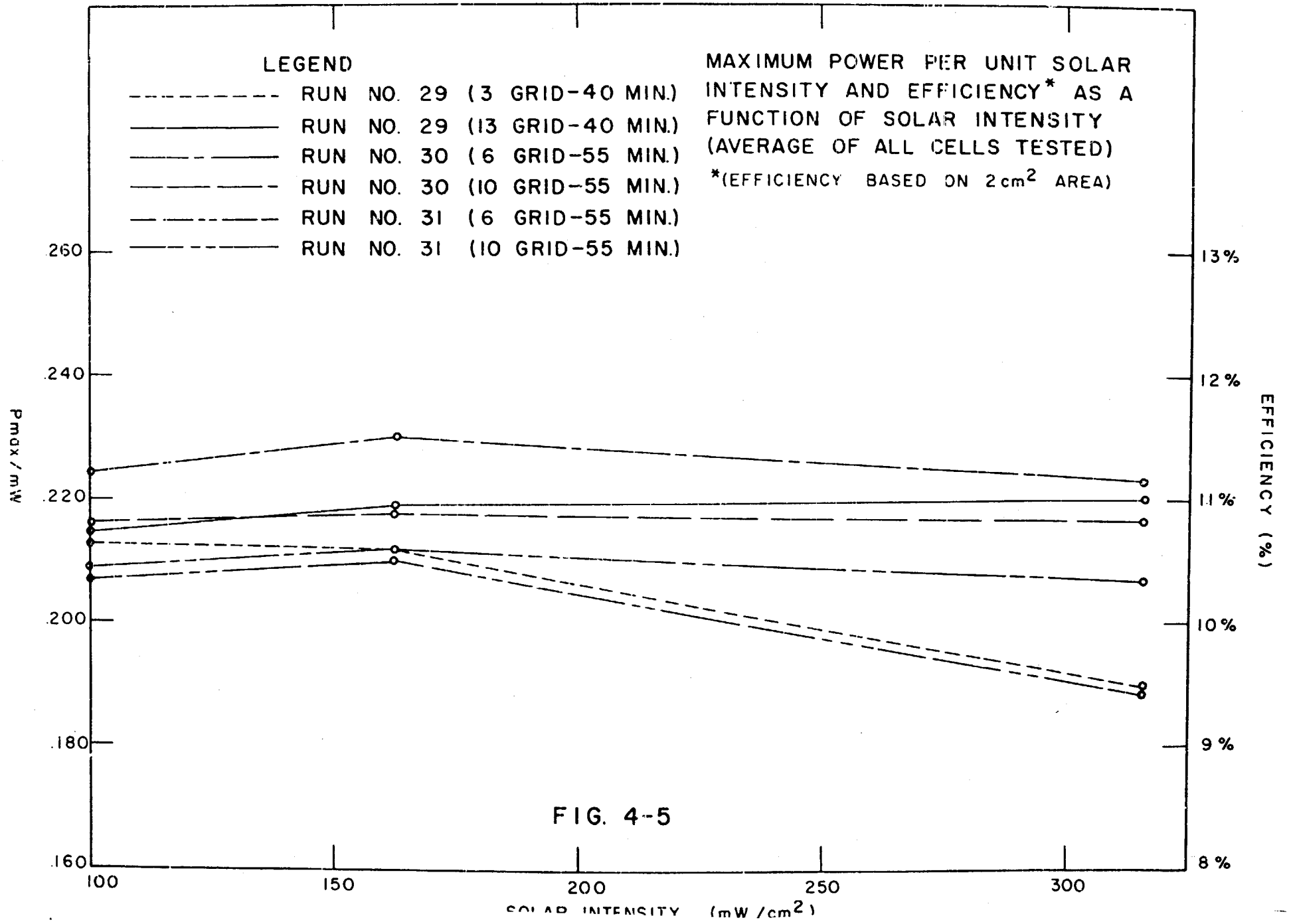
LEGEND
RUN NO. 29 (3 GRID-40 MIN.)
RUN NO. 29 (13 GRID-40 MIN.)
RUN NO. 30 (6 GRID-55 MIN.)
RUN NO. 30 (10 GRID-55 MIN.)
RUN NO. 31 (6 GRID-55 MIN.)
RUN NO. 31 (10 GRID-55 MIN.)
MAXIMUM POWER PER UNIT SOLAR INTENSITY AND EFFICIENCY* AS A FUNCTION OF SOLAR INTENSITY (AVERAGE OF ALL CELLS TESTED)
*(EFFICIENCY BASED ON 2 cm² AREA)
Pmax / mW
.260
.240
.220
.200
.180
.160
EFFICIENCY (%)
13%
12%
11%
10%
9%
8%
100
150
200
250
300
SOLAR INTENSITY (mW / cm²)

FIG. 4-5

T-2114

FIG. 4-6

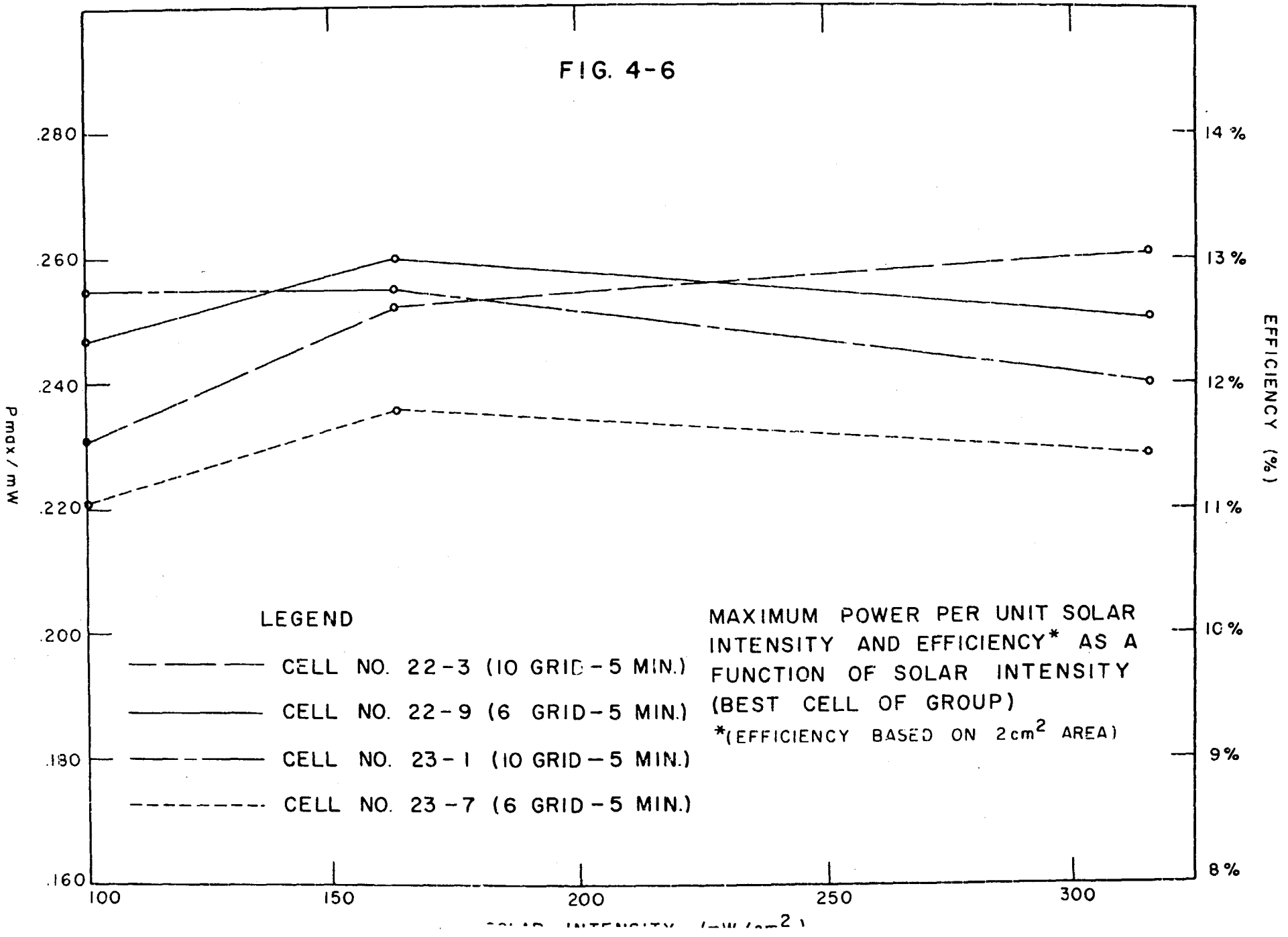
.280
.260
.240
.220
.200
.180
.160
Pmax / mW
14 %
13 %
12 %
11 %
10 %
9 %
8 %
EFFICIENCY (%)
100
150
200
250
300
LEGEND
CELL NO. 22-3 (10 GRID-5 MIN.)
CELL NO. 22-9 (6 GRID-5 MIN.)
CELL NO. 23-1 (10 GRID-5 MIN.)
CELL NO. 23-7 (6 GRID-5 MIN.)
MAXIMUM POWER PER UNIT SOLAR INTENSITY AND EFFICIENCY* AS A FUNCTION OF SOLAR INTENSITY (BEST CELL OF GROUP)
*(EFFICIENCY BASED ON 2cm² AREA)

T-2115

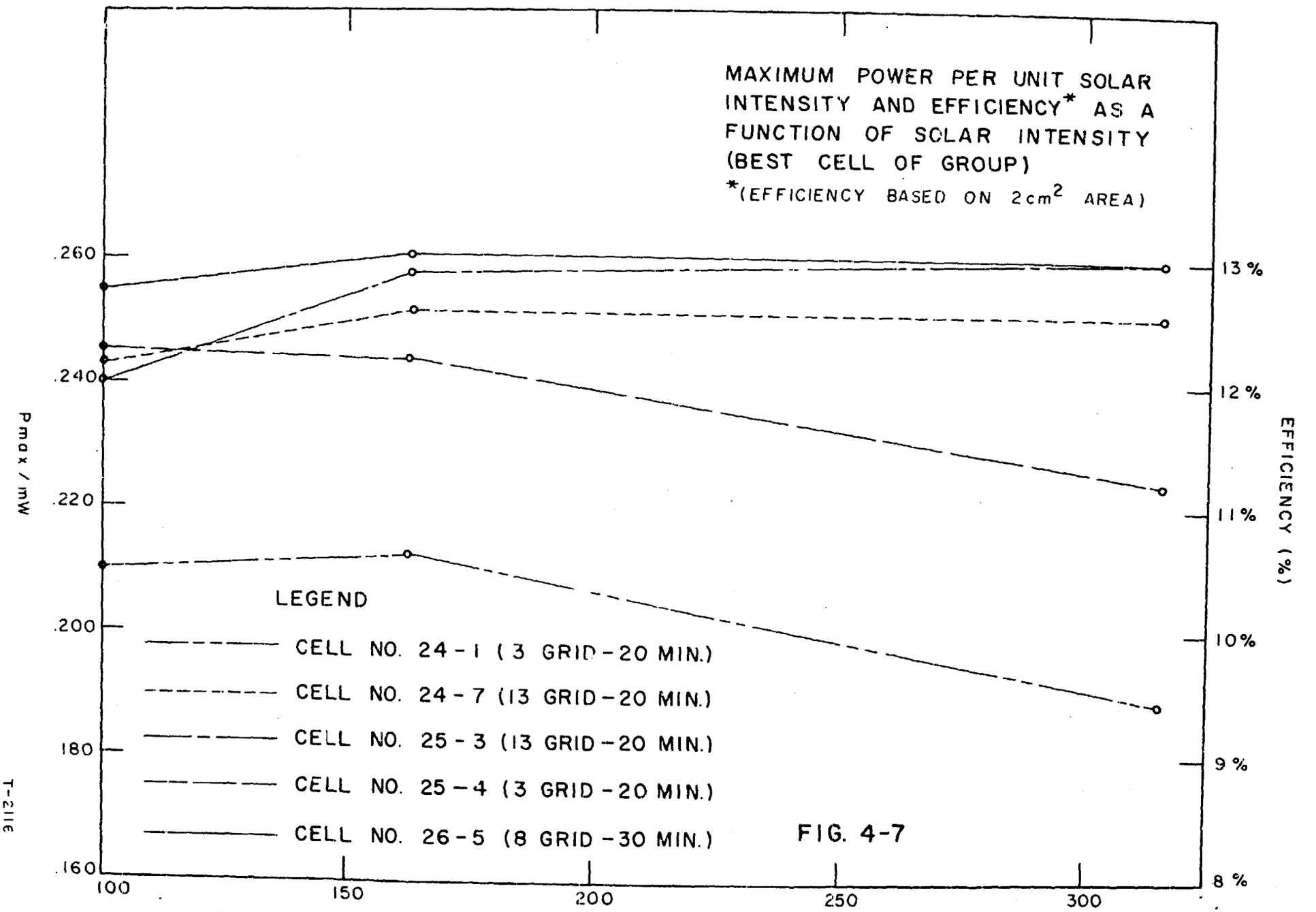
MAXIMUM POWER PER UNIT SOLAR INTENSITY AND EFFICIENCY* AS A FUNCTION OF SOLAR INTENSITY (BEST CELL OF GROUP)
*(EFFICIENCY BASED ON 2cm² AREA)
.260
.240
.220
.200
.180
.160
Pmax / mW
100
150
200
250
300
13 %
12 %
11 %
10 %
9 %
8 %
EFFICIENCY (%)
LEGEND
CELL NO. 24-1 (3 GRID-20 MIN.)
CELL NO. 24-7 (13 GRID-20 MIN.)
CELL NO. 25-3 (13 GRID-20 MIN.)
CELL NO. 25-4 (3 GRID-20 MIN.)
CELL NO. 26-5 (8 GRID-30 MIN.)

FIG. 4-7

T-2116

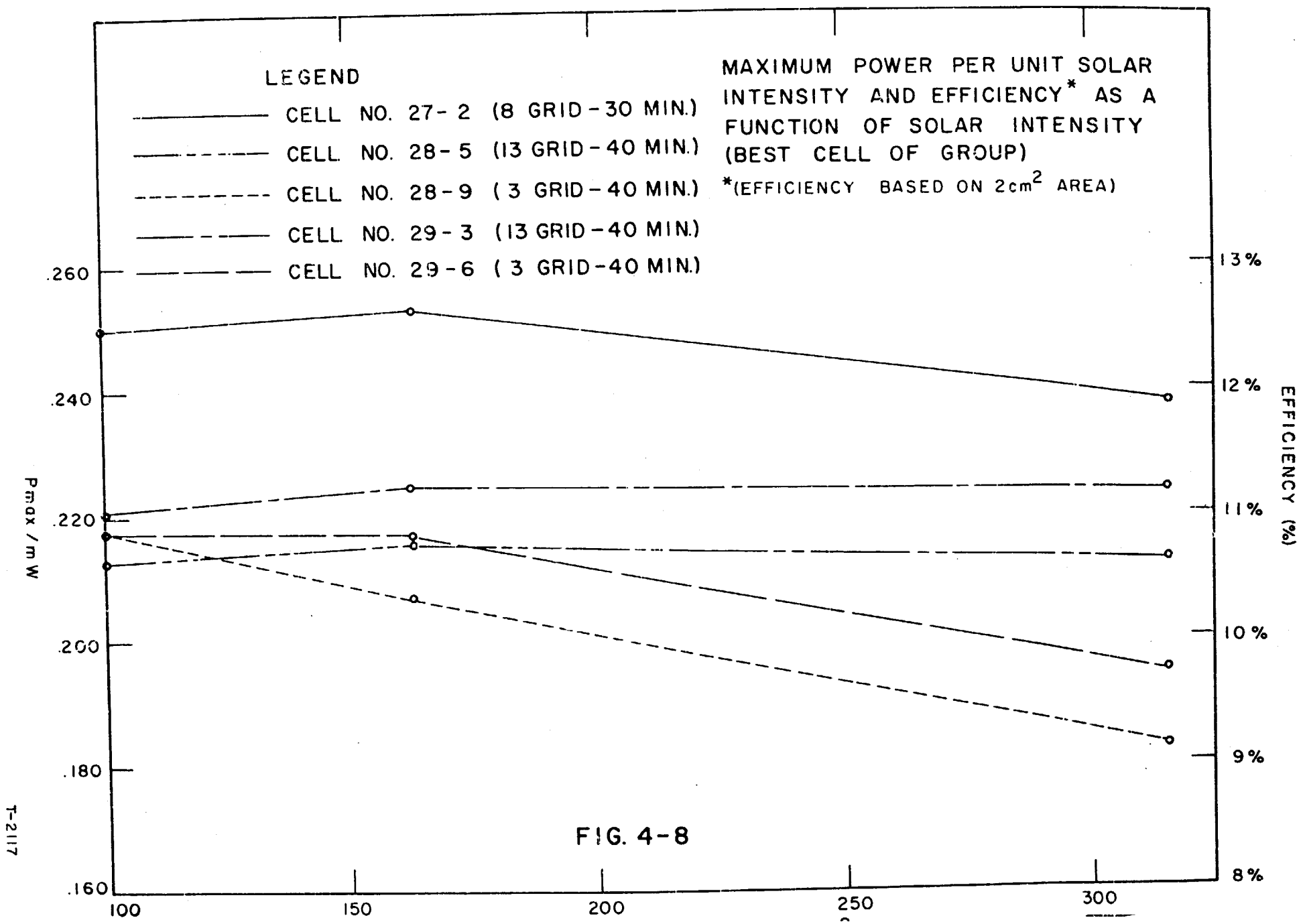
LEGEND
CELL NO. 27-2 (8 GRID-30 MIN.)
CELL NO. 28-5 (13 GRID-40 MIN.)
CELL NO. 28-9 (3 GRID-40 MIN.)
CELL NO. 29-3 (13 GRID-40 MIN.)
CELL NO. 29-6 (3 GRID-40 MIN.)
MAXIMUM POWER PER UNIT SOLAR INTENSITY AND EFFICIENCY* AS A FUNCTION OF SOLAR INTENSITY (BEST CELL OF GROUP)
*(EFFICIENCY BASED ON 2cm² AREA)
Pmax / mW
.260
.240
.220
.200
.180
.160
EFFICIENCY (%)
13%
12%
11%
10%
9%
8%
100
150
200
250
300

FIG. 4-8

T-2117

Run Number	Diffusion Time (minutes)
22	5
23	5
24	20
25	20
26	30
27	30
28	40
29	40
30	55
31	55

The highest cell efficiencies at the 316 mW/cm^2 light intensity occurred for the 10 gridded-5 minute diffused cells and the 13 gridded-20 minute diffusions. The behavior of the 5 minute diffused cells in Run No. 22 is somewhat better than what was expected but was not consistent with the results obtained from the 10 gridded-5 minute diffused cells of Run No. 23 since the curve appropriate to the former cells is still increasing at 316 mW/cm^2 input, while that of the latter cells appears to be decreasing. This indicates that another variable is probably affecting the results. In general, cells diffused for 40 minutes or longer do not seem to be advantageous for concentration use due to the severe loss of response to light in the 6000 Å wavelength region.

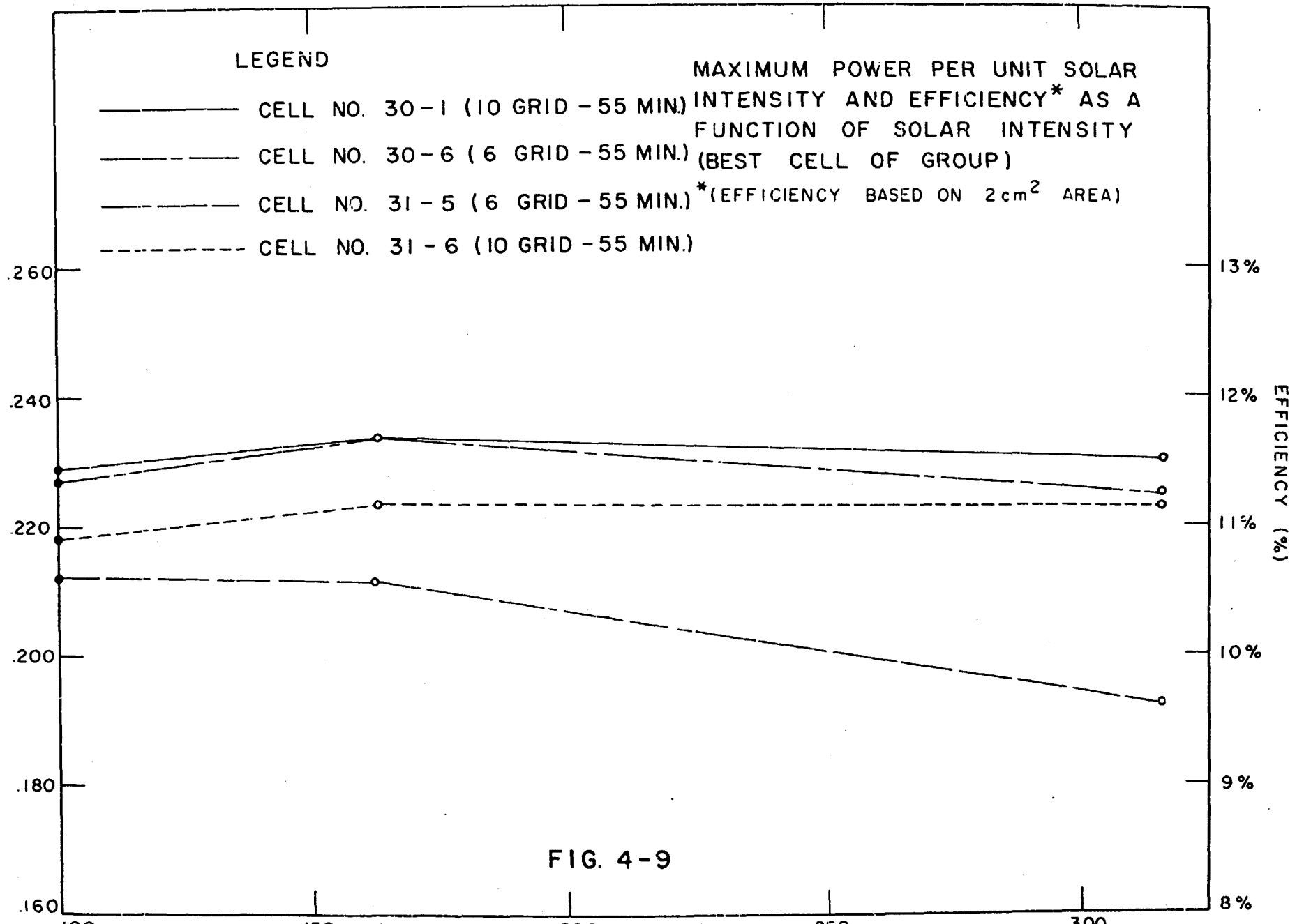
LEGEND
CELL NO. 30-1 (10 GRID - 55 MIN.)
CELL NO. 30-6 (6 GRID - 55 MIN.)
CELL NO. 31-5 (6 GRID - 55 MIN.)
CELL NO. 31-6 (10 GRID - 55 MIN.)
MAXIMUM POWER PER UNIT SOLAR INTENSITY AND EFFICIENCY* AS A FUNCTION OF SOLAR INTENSITY (BEST CELL OF GROUP)
*(EFFICIENCY BASED ON 2 cm² AREA)
Pmax / mW
.260
.240
.220
.200
.180
.160
EFFICIENCY (%)
13%
12%
11%
10%
9%
8%
100
150
200
250
300

FIG. 4-9

T-2118

5.0 COST FACTORS

In the First Quarterly Progress Report the use of polycrystalline material in solar cell fabrication was discussed as a possible method of reducing solar cell cost.

Experimentation in the fabrication of solar cells utilizing polycrystalline base material has been continued during this period. The cells fabricated from N-type polycrystalline material of approximately 1 ohm-cm resistivity exhibited spectral responses which peaked at a wavelength of about 0.73 microns, whereas standard N^+/P and P^+/N cells fabricated from single crystalline material normally peak at a wavelength of about 0.85 microns. These values are based on a constant energy input at each of the wavelengths measured. This phenomenon was expected since the polycrystalline grain boundaries introduce a large number of energy levels in the forbidden gap, and many of these traps act as recombination centers, reducing the lifetime of the minority carriers in the base region of the solar cell. This reduces the long wavelength response of the cell so that the peak response occurs at shorter wavelengths than for single crystalline cells. The response from the diffused region is not greatly affected by the additional recombination centers introduced by the polycrystalline grain boundaries because many recombination centers already exist, due to the degeneracy of the region. Thus carrier collection from the diffused region is relatively independent of further minority carrier lifetime reduction. Instead junction collection from the diffused region depends primarily upon the creation of the minority carrier in the space charge region of the junction or in very close proximity to the junction so that the electronic field, which exists because of the large impurity gradient in the diffused region, accelerates these carriers to the junction before recombination can occur. An example of the spectral response of a P^+/N polycrystalline solar cell is shown in Fig. 5 - 1. This spectral response corresponds to a significant decrease in the red response thus making the cell relatively more blue sensitive with

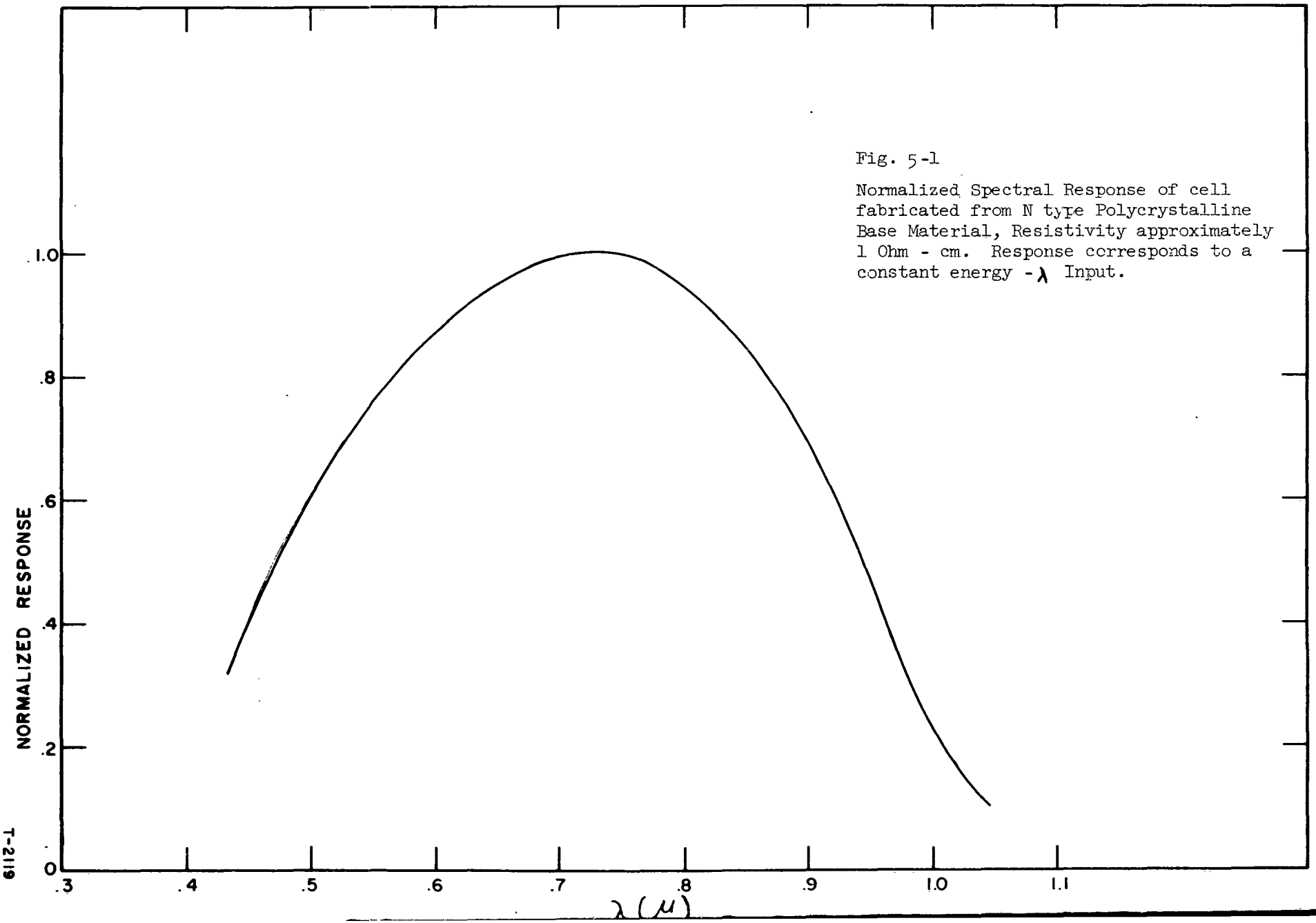

Fig. 5-1

Normalized Spectral Response of cell fabricated from N type Polycrystalline Base Material, Resistivity approximately 1 Ohm - cm. Response corresponds to a constant energy - λ Input.

respect to the typical cell made commercially. Since the typical commercial type cell is used to standardize the tungsten light sources (which consists of much more long wavelength light than sunlight) to correspond to 100 mW/cm^2 of sunlight, it would be expected that these polycrystalline cells would exhibit higher efficiencies in sunlight than in tungsten light. This was found to be the case when these cells were measured both in tungsten light and in natural sunlight at Table Mountain, California as shown below:

Cell Identification Number	Number of Grid Stripes	Power Tungsten Light = 100 mW/cm^2 (mW)	Power Sunlight M=1 at 100 mW/cm^2 (mW)	Eff. (%) Sunlight M=1 Based on 2cm^2 Area
81-1	5	12.5	16.6	8.3
81-2	5	12.3	16.2	8.1
82-1	8	13.8	18.6	9.3
82-2	8	11.4	13.7	6.9

It should be pointed out that the efficiencies shown are based on a 2 cm^2 area, whereas it is common in the industry to subtract off a portion of the area of the contacts in computing the efficiency; thus, for example the area of these cells would be considered as 1.8 cm^2, giving rise to an efficiency in sunlight of 10.2% for the best cell. In this case cells having 5 and 8 grid lines were studied to evaluate the effects of more grid lines on polycrystalline cells. It is not clear which grid configuration is more advantageous from these results, although the cell having the highest efficiency, 9.3%, (based on 2 cm^2 area) in sunlight has 8 grid lines.

Cells were also fabricated from P-type polycrystalline material having a resistivity of about 7 ohm-cm. Cells fabricated from this material were diffused for 20 minutes and 45 minutes to determine the effect of

diffused layer thickness on cell performance. Figures 5 - 2 and 5 - 4 show normalized spectral responses of cells diffused for 20 minutes and 45 minutes respectively. Little difference is seen between the responses of these two cells, the relative red response being almost identical and a slight increase in blue response occuring surprisingly enough, in the deeper diffused cell. In Fig. 5 - 3 is presented the response of a 20 minute diffused N^+/P polycrystalline cell with a silicon monoxide anti-reflectance coating applied. Little difference in relative response is seen between the coated and uncoated cells which indicates the coating is not particularly selective in wavelength response. In general, the responses of the N^+/P cells were significantly different from the P^+/N cells, the former cell type exhibiting more red response, although both cell types showed peak response in the 0.73 - 0.75 μ wavelength region. The increased red response is most likely due to the higher resistivity, and hence higher minority carrier lifetime of the P-type polycrystalline material.

The power output of the N^+/P cells have been measured under tungsten light having a color temperature of 2800°K at a cell temperature of 28°C ± 2°C. The following results were obtained:

Diffusion Time (Minutes)	Number of Grid Lines	Coating	V_{oc} Avg. (Volts)	I_{sc} Avg. (mA)	P Max. Avg. (mW)	Effic. Avg. Based on 2 cm^2 Area (%)
20	5	S_iO	.487	43.6	15.0	7.5
20	10	S_iO	.493	42.1	14.8	7.4
20	5	None	.488	42.0	13.7	6.8
20	10	None	.475	43.2	13.3	6.6
45	5	None	.449	40.9	11.1	5.5
45	10	None	.436	41.0	11.5	5.7

In general, it seems that for the 20-minute diffused cells the 5-line grid pattern gives rise to higher efficiency cells. The 10-line grid

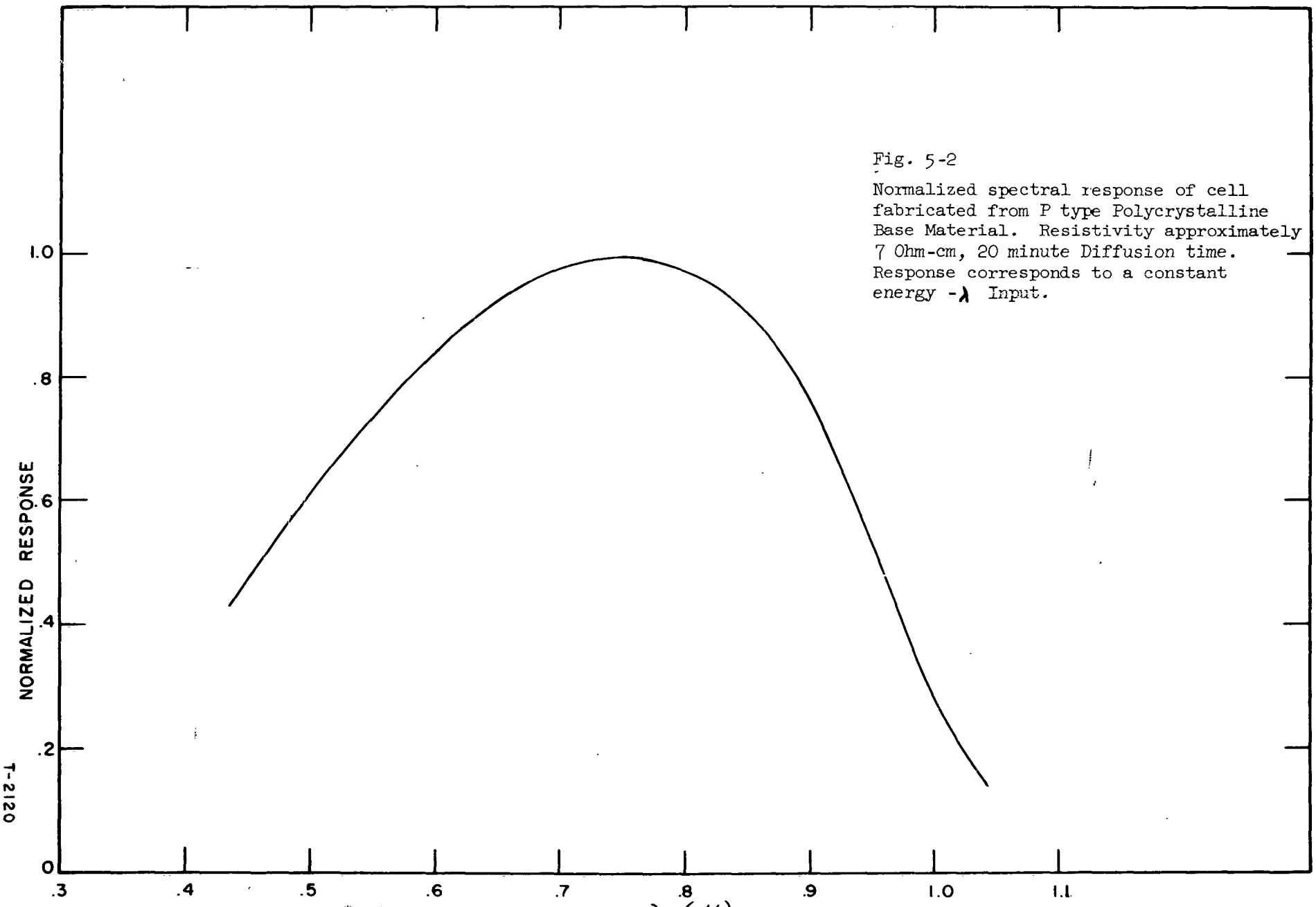

Fig. 5-2

Normalized spectral response of cell fabricated from P type Polycrystalline Base Material. Resistivity approximately 7 Ohm-cm, 20 minute Diffusion time. Response corresponds to a constant energy -λ Input.

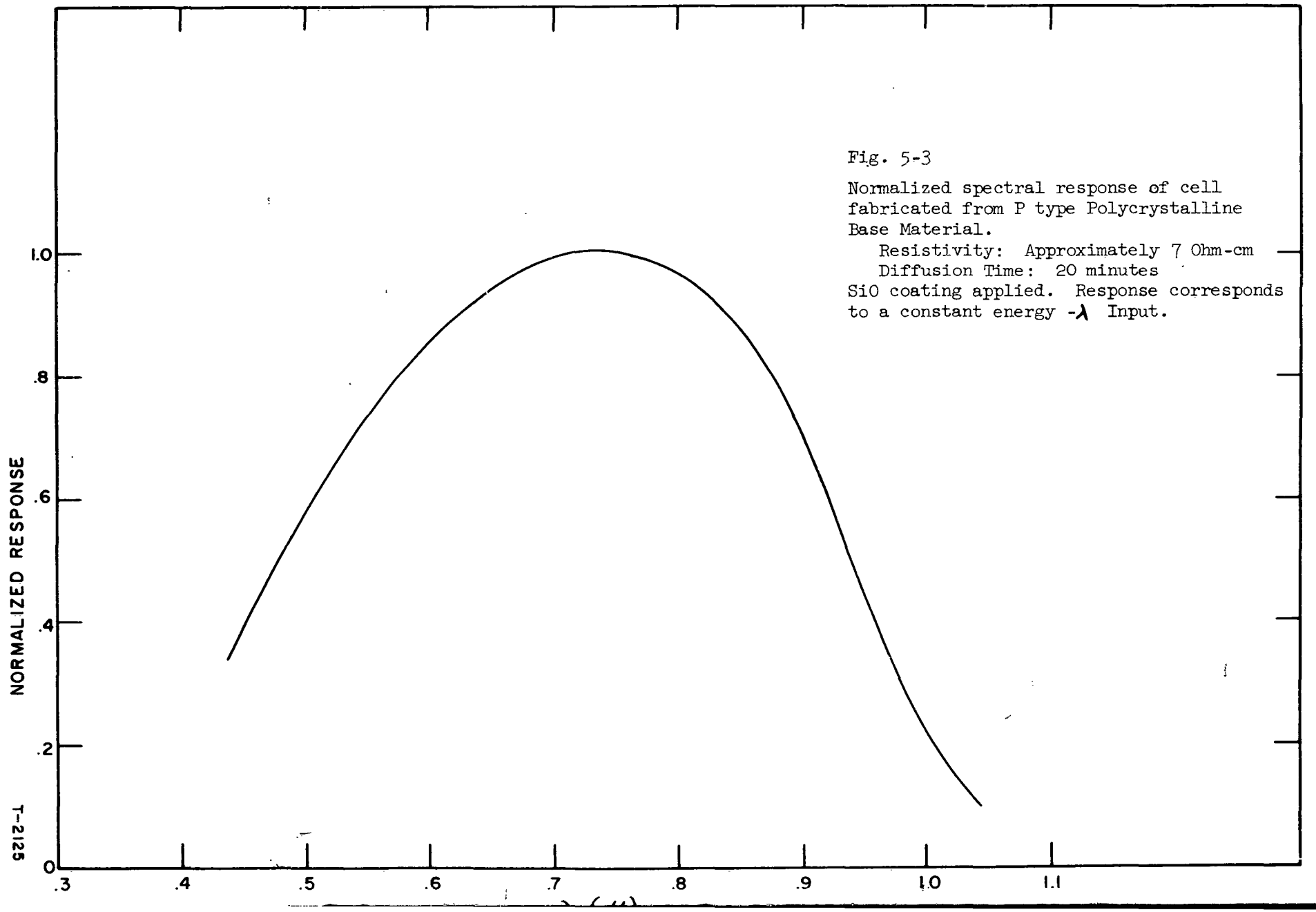

Fig. 5-3

Normalized spectral response of cell fabricated from P type Polycrystalline Base Material.

Resistivity: Approximately 7 Ohm-cm
Diffusion Time: 20 minutes

SiO coating applied. Response corresponds to a constant energy -λ Input.

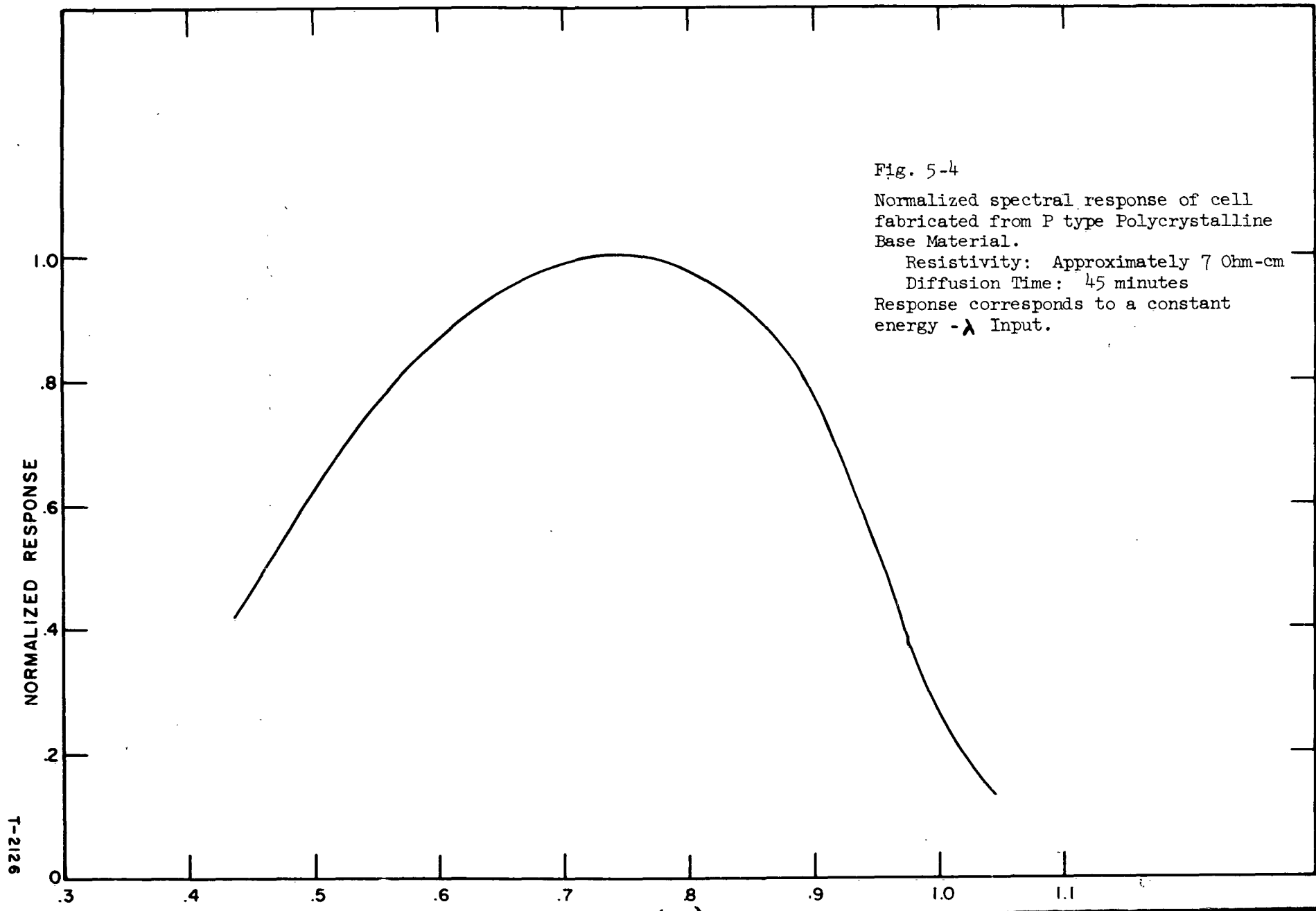

Fig. 5-4

Normalized spectral response of cell fabricated from P type Polycrystalline Base Material.

Resistivity: Approximately 7 Ohm-cm
Diffusion Time: 45 minutes

Response corresponds to a constant energy - λ Input.

pattern gives rise to higher open circuit voltages, which might be expected because of the more efficient separation of the polycrystalline grain boundaries by the grid stripes. The cells which were silicon monoxide coated gave, oddly enough, no significant increase in short circuit current as it does in the normal single crystal type cell, but the average power output of these cells was higher than the uncoated cells. This latter fact may be completely coincidental, since there was considerably more shunting effect in the uncoated cells as observed from the current voltage curves, indicating that the lower efficiencies might have been due to processing.

The 45-minute diffused cells showed the lowest power output, the open circuit voltages being considerably lower than those of the 20-minute diffused cells. In cells fabricated from single crystalline material the reverse is usually true. That is, deeper diffused cells usually have open circuit voltages equal to or greater than shallow diffused cells. However, in the case of polycrystalline cells the impurity diffusion might be expected to propagate much more rapidly down the grain boundaries than through the single crystalline areas, reducing the open circuit voltage by introducing thin spikes or shunting paths of diffused impurities deep into the bulk region of the cells.

Because the N^+/P polycrystalline cells have more response in the red region than the P^+/N cells, it is to be expected that the power increase in sunlight over that in tungsten light would not be as great for the former cell type as the latter. Time has not permitted verification of this as yet.

The results of the polycrystalline experiments have continued to look quite promising and the achievement of an efficiency of over 10% in sunlight is significant. Further work in this area is obviously indicated.

6.0 ENVIRONMENTAL TESTS

In order for solar cells to be useful as sources of power on earth or in space the cells should experience a minimum power degradation after exposure to rather severe environmental conditions. For terrestrial use, cells should be capable of operating efficiently in extreme desert heat or arctic cold. The necessity of operating at elevated temperatures may be even more pressing if the cells are to be used in concentrator systems where no cooling is available. It is therefore necessary to subject cells representative of the state-of-the-art to environmental conditions more severe than they would normally encounter, the two most representative tests being extreme heat and extreme cold. It is well known that exposure to heat over a period of time degrades some semiconductor devices while prolonged exposure to extreme cold seems to have little effect beyond the initial degradations which usually occur during the transition between room temperature and the soak temperature, due to mismatches in the expansion coefficients of the various component parts of the device. For a semiconductor device, a far more significant test than a low temperature soak would be a series of thermal cycles in which the temperature of the device would be varied between some temperature above room ambient and the desired low temperature extreme. With this in mind, the following tests were performed in order to give some indication of the capabilities of the various cell types with respect to temperature stress.

A high temperature soak or life test was performed which consisted of simultaneous exposure of 50 N^+/P cells having an efficiency of 12% and 50 P^+/N cells having an efficiency of 13% to an ambient temperature of 155°C for a period of 168 hours. Ten control cells of each type which did not go through the test were measured along with the tested cells. The temperature was checked manually seven times each day.

As a result of the test the N^+/P cells experienced a mean current improvement at a voltage of 0.4 Volts of 1.1 mA with a standard deviation of 1.2 mA, while the N^+/P control cells (which did not go through the environmental test) showed a degradation of 0.1 mA with a standard deviation of 0.2 mA. The P^+/N cells experienced a mean current degradation at a voltage of 0.48 Volts of 6.0 mA with a standard deviation of 2.8 mA, while the P^+/N control cells exhibited a degradation of 0.2 mA with a standard deviation of 0.5 mA. The currents were measured at voltages of 0.4 and 0.48 for N^+/P and P^+/N cells respectively because these are near the statistically observed maximum power voltages for the respective cell types.

The effects of the test on the electrical characteristics of the cells are quite interesting since there is a distinct difference in results between the cell types. The N^+/P cells exhibited very minute changes in power output at 0.4 Volts (actually an increase was observed) while the P^+/N cells showed a significant degradation in power at 0.48 Volts which represented about a 10% decrease at this voltage.

A series of temperature cycle experiments was performed on 50 12% efficient N^+/P type cells during which the cell temperatures were cycled between +62°C to -83°C. The cycling was performed by placing the cells on a hot-plate which was maintained at 62°C ± 3°C until temperature equilibrium was established. Then the cells were placed directly into a dry ice-acetone bath (-83°C ± 3°C) until temperature equilibrium again was attained, so that the cells actually underwent more of a thermal shock than a cycle. After four hundred cycles the mean maximum power degradation was 5.6% with a standard deviation of 3.8%, while the mean degradation in maximum power of the nine control cells, which were not subjected to the temperature cycle tests, was 1.9% with a standard deviation of 1.6%. The mean current degradation at 0.43 Volts was 2.7 mA with a standard deviation of 1.8 mA, while the control cells degraded 0.6 mA with a standard deviation of 0.7 mA.

After the cells had undergone a total of 800 temperature cycles the total mean degradation (as compared to the measurements made prior to any cycling) of maximum power was 7% with a standard deviation of 5% while the mean maximum power degradation of the control cells was 1% with no significant standard deviation. The total mean current degradation at a voltage of 0.43 Volts was 3.1 mA with a standard deviation of 2.3 mA while the total current degradation of the control cells at 0.43 Volts was 0.2 mA with a standard deviation of 0.8 mA.

The results of the test seem to indicate that the power degradation experienced after the second series of 400 cycles was quite similar to that experienced after the first 400 cycles, though the degradation may be somewhat less severe during the second series. After control cell corrections are made the total degradation in maximum power and power at 0.43 Volts is about 4.8% and 5.6% respectively for the entire series of 800 temperature cycles. The conclusion that can be made is that very severe environmental stresses in the form of temperature extremes can be experienced with little degradation. Therefore either the N^+/P or the P^+/N type solar cell should be equally adjusted for terrestrial use from this standpoint.

7.0 CONCLUSIONS

The results of the preliminary experiments on the behavior of cells having various junction depths under concentrated solar intensities of approximately 300 mW/cm^2 has been verified by two additional experiments. If all other parameters remain constant, the cells diffused for twice the length of time as production type cells have higher efficiencies at 300 mW/cm^2 solar intensities than the production type cells. The P^+/N type cells were more efficient at the concentrated intensities than the N^+/P cells, probably due to the lower resistivity material used to fabricate the former cell type. Various methods of cross-checking these results were employed and good agreement was obtained.

The results of the polyvariable experiment will be analyzed by means of a computer.

A preliminary evaluation of the results indicate that there is no obvious optimum value for the parameters. Instead it appears that over the intensity range being studied the variations in the results are not significantly larger than the variations that one obtains due to random process fluctuations. Therefore, in several of the experimental runs the actual parameters being studied are partially masked.

Contact resistance at the base contact of N^+/P cells can become as large as .5 ohm if base material of about 20 ohm centimeters is used. For lower resistivity material, below about 10 ohms per centimeter, the contact resistance can be reduced to about 0.08 ohms. The contact resistance to the diffused layer of both N^+/P and P^+/N cells can be neglected for this study.

The spectral response of cells fabricated from polycrystalline material peaks at a wavelength of about 0.73μ due to the low minority carrier

lifetime in the base region of the cell. Deeper diffused polycrystalline cells have lower efficiencies than shallower diffused cells, the loss being mainly in open circuit voltage. Polycrystalline cells having sunlight efficiencies greater than 9% in sunlight can be made.

PROGRAM FOR NEXT INTERVAL

The results of the first bivariable experiment as described in this report will be sent to U. S. Army Electronics Research and Development Laboratory for evaluation and determination of the optimum parameters by means of computer analysis. If time permits, a repeat set of experiments will be done for basis of comparison and verification of the first set. A similar polyvariable experiment will be performed utilizing N^+/P cells fabricated from low resistivity (approximately 1 ohm-cm) material.

Other studies to be continued during the next period are: improvement of efficiency of cells fabricated from polycrystalline silicon base material, improvement of cell contacts in order to decrease series resistance and improve reliability of mechanical strength, and theoretical optimization of the number of grids and geometrical configuration of cells.

IDENTIFICATION OF KEY TECHNICAL PERSONNEL

The following engineering hours of work were performed during this reporting period.

M. Wolf	107 hours
E. Ralph	274 hours
P. Berman	472 hours
R. Handy	54 hours
G. Rolik	160 hours
S. vonSzeremy	70 hours
T. Downey	24 hours

There were also 664 hours of work performed by various other Heliot.. personnel, such as Engineering Aides, Technicians and Draftsmen in collecting and presenting the data contained in this report.

A brief resume of Mr. Downey's background that was not included in the first quarterly report is added on the following page.

James T. Downey, Engineer, Device Development

Born in Los Angeles, California, he attended grade and high schools at Bishop, California and went on to engineering studies at San Fernando Valley College, North Hollywood, California.

From 1956 to 1961 he was employed by Bendix Corporation, North Hollywood, California where he was primarily responsible for test equipment design and manufacture in the Sonar, Radar and Telemetry fields. He was also involved with programming and evaluation of automatic production test equipment in these fields.

He joined Heliotek, Division of Textron Electronics, Inc., Sylmar, California, in 1961 where his responsibilities are the testing of various types of special solar cells, along with the design and fabrication of related test equipment.

AD_____Accession No._____

Heliotek, Division of Textron Electronics, Inc.
12500 Gladstone Avenue
Sylmar, California
HIGH EFFICIENCY SILICON SOLAR CELLS
Paul A. Berman, Roland J. Handy, and Geza P. Rolik

Second Quarterly Report, September 15, 1962 to December 15, 1962
Signal Corps Contract DA 36-039-SC-90777
Order No. 1091-PM-62-93-93(4213), Unclassified Report

Work on the effect of concentrated sunlight on the performance of solar cells has been continued. Once again cells which were diffused for twice the length of time as the standard production cells exhibited better performance under 300 mW/cm^2 solar intensity when all other parameters were held constant. The series resistance of the deeper diffused type cell was several tenths of an ohm lower than the shallow diffused type cell.

Actual values of diffused sheet resistance, bulk resistance, contact resistance to the diffused layer electrodes, and contact resistance to the bulk electrodes have been experimentally determined for N^+/P and P^+/N type cells. A theoretical method has been developed for the determination and isolation of the resistance of the silicon for carriers flowing to the contact strip and for carriers flowing to the grid strip. These resistances can be determined from a knowledge of the resistivity of the diffused sheet and the physical dimensions of the cell.

Cells of N^+/P and P^+/N polarity have been fabricated from polycrystalline base material. Representative spectral response curves are presented. A P^+/N polycrystalline cell having an efficiency in sunlight (m=1) of greater than 9% has been fabricated. Various diffusion depths and grid patterns are considered with respect to polycrystalline cell performance.

A polyvariable experiment has been carried out in an attempt to determine the optimum diffusion time and number of grid stripes for P^+/N cells to be operated at a solar intensity of about 300 mW/cm^2.

Improved contacting techniques are considered in order to decrease series resistance and improve high temperature performance.

UNCLASSIFIED

1. Solar Energy Converters (Solar Batteries)
2. Effect of High Concentration Ratios on Silicon Solar Cells
3. Signal Corps Contract DA 36-039-SC-90777

AD_____Accession No._____

Heliotek, Division of Textron Electronics, Inc.
12500 Gladstone Avenue
Sylmar, California
HIGH EFFICIENCY SILICON SOLAR CELLS
Paul A. Berman, Roland J. Handy, and Geza P. Rolik

Second Quarterly Report, September 15, 1962 to December 15, 1962
Signal Corps Contract DA 36-039-SC-90777
Order No. 1091-PM-62-93-93(4213), Unclassified Report

Work on the effect of concentrated sunlight on the performance of solar cells has been continued. Once again cells which were diffused for twice the length of time as the standard production cells exhibited better performance under 300 mW/cm^2 solar intensity when all other parameters were held constant. The series resistance of the deeper diffused type cell was several tenths of an ohm lower than the shallow diffused type cell.

Actual values of diffused sheet resistance, bulk resistance, contact resistance to the diffused layer electrodes, and contact resistance to the bulk electrodes have been experimentally determined for N^+/P and P^+/N type cells. A theoretical method has been developed for the determination and isolation of the resistance of the silicon for carriers flowing to the contact strip and for carriers flowing to the grid strip. These resistances can be determined from a knowledge of the resistivity of the diffused sheet and the physical dimensions of the cell.

Cells of N^+/P and P^+/N polarity have been fabricated from polycrystalline base material. Representative spectral response curves are presented. A P^+/N polycrystalline cell having an efficiency in sunlight (m=1) of greater than 9% has been fabricated. Various diffusion depths and grid patterns are considered with respect to polycrystalline cell performance.

A polyvariable experiment has been carried out in an attempt to determine the optimum diffusion time and number of grid stripes for P^+/N cells to be operated at a solar intensity of about 300 mW/cm^2.

Improved contacting techniques are considered in order to decrease series resistance and improve high temperature performance.

UNCLASSIFIED

1. Solar Energy Converters (Solar Batteries)
2. Effect of High Concentration Ratios on Silicon Solar Cells
3. Signal Corps Contract DA 36-039-SC-90777

AD_____Accession No._____

Heliotek, Division of Textron Electronics, Inc.
12500 Gladstone Avenue
Sylmar, California
HIGH EFFICIENCY SILICON SOLAR CELLS
Paul A. Berman, Roland J. Handy, and Geza P. Rolik

Second Quarterly Report, September 15, 1962 to December 15, 1962
Signal Corps Contract DA 36-039-SC-90777
Order No. 1091-PM-62-93-93(4213), Unclassified Report

Work on the effect of concentrated sunlight on the performance of solar cells has been continued. Once again cells which were diffused for twice the length of time as the standard production cells exhibited better performance under 300 mW/cm^2 solar intensity when all other parameters were held constant. The series resistance of the deeper diffused type cell was several tenths of an ohm lower than the shallow diffused type cell.

Actual values of diffused sheet resistance, bulk resistance, contact resistance to the diffused layer electrodes, and contact resistance to the bulk electrodes have been experimentally determined for N^+/P and P^+/N type cells. A theoretical method has been developed for the determination and isolation of the resistance of the silicon for carriers flowing to the contact strip and for carriers flowing to the grid strip. These resistances can be determined from a knowledge of the resistivity of the diffused sheet and the physical dimensions of the cell.

Cells of N^+/P and P^+/N polarity have been fabricated from polycrystalline base material. Representative spectral response curves are presented. A P^+/N polycrystalline cell having an efficiency in sunlight (m=1) of greater than 9% has been fabricated. Various diffusion depths and grid patterns are considered with respect to polycrystalline cell performance.

A polyvariable experiment has been carried out in an attempt to determine the optimum diffusion time and number of grid stripes for P^+/N cells to be operated at a solar intensity of about 300 mW/cm^2.

Improved contacting techniques are considered in order to decrease series resistance and improve high temperature performance.

UNCLASSIFIED

1. Solar Energy Converters (Solar Batteries)
2. Effect of High Concentration Ratios on Silicon Solar Cells
3. Signal Corps Contract DA 36-039-SC-90777

AD_____Accession No._____

Heliotek, Division of Textron Electronics, Inc.
12500 Gladstone Avenue
Sylmar, California
HIGH EFFICIENCY SILICON SOLAR CELLS
Paul A. Berman, Roland J. Handy, and Geza P. Rolik

Second Quarterly Report, September 15, 1962 to December 15, 1962
Signal Corps Contract DA 36-039-SC-90777
Order No. 1091-PM-62-93-93(4213), Unclassified Report

Work on the effect of concentrated sunlight on the performance of solar cells has been continued. Once again cells which were diffused for twice the length of time as the standard production cells exhibited better performance under 300 mW/cm^2 solar intensity when all other parameters were held constant. The series resistance of the deeper diffused type cell was several tenths of an ohm lower than the shallow diffused type cell.

Actual values of diffused sheet resistance, bulk resistance, contact resistance to the diffused layer electrodes, and contact resistance to the bulk electrodes have been experimentally determined for N^+/P and P^+/N type cells. A theoretical method has been developed for the determination and isolation of the resistance of the silicon for carriers flowing to the contact strip and for carriers flowing to the grid strip. These resistances can be determined from a knowledge of the resistivity of the diffused sheet and the physical dimensions of the cell.

Cells of N^+/P and P^+/N polarity have been fabricated from polycrystalline base material. Representative spectral response curves are presented. A P^+/N polycrystalline cell having an efficiency in sunlight (m=1) of greater than 9% has been fabricated. Various diffusion depths and grid patterns are considered with respect to polycrystalline cell performance.

A polyvariable experiment has been carried out in an attempt to determine the optimum diffusion time and number of grid stripes for P^+/N cells to be operated at a solar intensity of about 300 mW/cm^2.

Improved contacting techniques are considered in order to decrease series resistance and improve high temperature performance.

UNCLASSIFIED

1. Solar Energy Converters (Solar Batteries)
2. Effect of High Concentration Ratios on Silicon Solar Cells
3. Signal Corps Contract DA 36-039-SC-90777

DISTRIBUTION LIST
SECOND QUARTERLY REPORT
CONTRACT NO. DA 36-039-SC-90777

Commanding Officer
U.S.A. Electronics Research and
Development Laboratory
Fort Monmouth, N. J.
ATTN: Logistics Division
(MARKED FOR PROJECT
ENGINEER) (9)
ATTN: SELRA/P (1)
ATTN: Dir of Research/Engineering (1)
ATTN: File Unit #1 (1)
ATTN: Technical Document Center (1)
ATTN: Technical Information Div.
(UNCLASSIFIED REPORTS ONLY
FOR RETRANSMITTAL TO
ACCREDITED BRITISH AND
CANADIAN GOVERNMENT
REPRESENTATIVES) (3)

OASD (R and D), Rm 3E1065
ATTN: Technical Library
The Pentagon
Washington 25, D. C. (1)

Chief of Research and Development
OCS, Department of the Army
Washington 25, D. C. (1)

Commanding General
U.S.A. Electronics Command
ATTN: AMSEL-AD
Fort Monmouth, N. J. (3)

Director
U.S. Naval Research Laboratory
ATTN: Code 2027
Washington 25, D. C. (1)

Commanding Officer and Director
U.S. Naval Electronics Laboratory
San Diego 52, California (1)

Air Force Cambridge Research
Laboratories
ATTN: CRZC
L. G. Hanscom Field
Bedford, Massachusetts (1)

Rome Air Development Center
ATTN: RAALD
Griffiss Air Force Base, N. Y. (1)

Commanding General
U.S.A. Electronics Research and
Development Activity
ATTN: Technical Library
Fort Huachuca, Arizona (1)

Commanding Officer
Harry Diamond Laboratories
ATTN: Library, Room 211, Bldg. 92
Connecticut Ave and Vann Ness St., N.W.
Washington 25, D. C. (1)

Commanding Officer
U.S.A. Electronics Material Support
Agency
ATTN: SELMS-ADJ
Fort Monmouth, N.J. (1)

Deputy President
U.S.A. Security Agency Board
Arlington Hall Station
Arlington 12, Virginia (1)

Commander
Armed Services Technical Information
Agency
ATTN: TISIA
Arlington Hall Station
Arlington 12, Virginia (10)

Chief
U.S.A. Security Agency
Arlington Hall Station
Arlington 12, Virginia (2)

Commander
Aeronautical Systems Division
ATTN: ASAPRL
Wright-Patterson Air Force Base
Ohio (1)

Air Force Cambridge Research
Laboratories
L. G. Hanscom Field
Bedford, Massachusetts (1)

DISTRIBUTION LIST
SECOND QUARTERLY REPORT
CONTRACT NO. DA 36-039-SC-90777

Headquarters
U.S. Army Materiel Command
Research and Development Directorate
ATTN: AMCRD-DE-MO
Washington 25, D. C. (1)

Commanding General
U.S.A. Electronics Command
ATTN: AMSEL-RE-A
Fort Monmouth, N. J. (1)

Commanding General
U.S.A. Combat Developments Command
ATTN: CDCMR-E
Fort Belvoir, Virginia (1)

Commanding Officer
U.S.A. Communications and Electronics
Combat Development Agency
Fort Huachuca, Arizona (1)

Director
Fort Monmouth Office
U.S.A. Communications and Electronics
Combat Development Agency
Fort Monmouth, N.J. (1)

Air Force Systems Command
Scientific/Technical Liaison Office
U.S. Naval Air Development Center
Johnsville, Pennsylvania (1)

Corps of Engineers Liaison Office
U.S.A. Electronics Research and
Development Laboratory
Fort Monmouth, N. J. (1)

Marine Corps Liaison Office
U.S.A. Electronics Research and
Development Laboratory
Fort Monmouth, N. J. (1)

AFSC Scientific/Technical Liaison Office
U.S.A. Electronics Research and
Development Laboratory
Fort Monmouth, N. J. (1)

Power Information Center
Moore School Building
200 South Thirty-Third Street
Philadelphia 4, Pennsylvania (1)

Dr. Sidney J. Magram
Physical Sciences Division
Army Research Office
3045 Columbia Pike
Arlington, Va. (1)

Dr. Ralph Roberts
Head, Power Branch
Office of Naval Research (Code 429)
Department of the Navy
Washington 25, D. C. (1)

Mr. Bernard B. Rosenbaum
Bureau of Ships (Code 340)
Department of the Navy
Washington 25, D.C. (1)

Mr. George W. Sherman
Aeronautical Systems Division
ATTN: ASRMFP
Wright-Patterson Air Force Base
Ohio (1)

Dr. John H. Huth
Advanced Research Projects Agency
The Pentagon, Room 3E157
Washington 25, D. C. (1)

Lt. Col. George H. Ogburn, Jr.
Auxiliary Power Branch (SNAP)
Division of Reactor Development
U.S. Atomic Energy Commission
Washington 25, D. C. (1)

Mr. Walter C. Scott
National Aeronautics and Space
Administration
1520 H. Street, N. W.
Washington 25, D. C. (1)

DISTRIBUTION LIST
SECOND QUARTERLY REPORT
CONTRACT NO. DA 36-039-SC-90777

Institute for Defense Analysis
1666 Connecticut Avenue, N. W.
Washington 25, D. C.
ATTN: Dr. George Szego (1)
ATTN: Mr. Robert Hamilton (1)

United Aircraft Corporation
Hamilton Standard Division
Broad Brook, Connecticut
ATTN: Mr. Wm. Michel (1)

Transitron Electronic Corp.
168-182 Albion Street
Wakefield, Mass.
ATTN: Mr. E. Brown (1)

Texas Instruments
Semiconductor Components Division
P. O. Box 5012
Dallas 22, Texas (1)

Radio Corporation of America
Defense Electronic Products
Front and Cooper Streets
Camden 2, New Jersey
ATTN: Contract Services (1)

International Rectifier Corp.
1521 East Grand Avenue
El Segundo, California (1)

Hoffman Electronics Corp.
1625 I Street, N. W.
Suite 1009
Washington, D. C. (1)

Boeing Airplane Company
Seattle, Washington
ATTN: Mr. R. W. Curran (1)

Goodrich-High Voltage
Astronautics, Inc.
Burlington, Mass.
ATTN: Mr. W. J. King (1)

National Aeronautics and Space
Administration
Chemistry and Energy Conversion
Division
Lewis Research Center
21000 Brookpark Road
Cleveland, Ohio
ATTN: Mr. J. Mandelkorn

Department of the Air Force
Aeronautical Systems Division
Wright-Patterson Air Force Base
Ohio
ATTN: Mr. Joseph F. Wise
ASRMFP-2

The Eagle-Picher Company
200 9th Ave., N. E.
Miami, Oklahoma

Bell Telephone Laboratories
Murray Hill, New Jersey
ATTN: Mr. U. B. Thomas

General Motors Corporation
Defense Research Laboratories
Santa Barbara, California
ATTN: Mr. John Werth